energies

MDPI

Article

Dimethyl Ether as a Compression Ignition Engine Fuel for Simultaneous NO_x and PM Reduction

Matthias Rollins, Juan Felipe Rodriguez, Bret C. Windom and Daniel B. Olsen *

Department of Mechanical Engineering, Colorado State University, Fort Collins, CO 80523, USA
* Correspondence: daniel.olsen@colostate.edu

Abstract

Dimethyl ether (DME) is a promising alternative fuel for compression ignition (CI) engines due to its potential to simultaneously reduce nitrogen oxides (NO_x) and particulate matter (PM) emissions while maintaining diesel-equivalent power. However, its combustion behavior under varying injection timing and exhaust gas recirculation (EGR) conditions remains insufficiently characterized for practical calibration. This study investigates the combustion, emissions, and performance of DME relative to diesel using a fully instrumented John Deere 6068CI550 single-cylinder research engine modified for high-pressure common-rail DME operation. Baseline tests were conducted at three ISO 8178 C1 steady-state modes with matched combustion phasing, load, and EGR to isolate fuel property effects. Injection timing and EGR sweeps were then performed at 1600 rpm and 50% load. Results show that DME produces 10–35% lower NO_x and orders-of-magnitude lower PM than diesel while maintaining comparable thermal efficiency. DME exhibits a single-stage premixed heat release structure with reduced peak apparent heat release rates and 4–5° shorter combustion durations than diesel. Stable combustion was sustained up to 55% EGR, beyond which incomplete combustion increased carbon monoxide (CO), total hydrocarbons (THC), and fuel consumption. Optimal low-emission operation occurred near CA50 ≈ 16° ATDC and EGR levels of 30–40%. These findings demonstrate DME's ability to mitigate the traditional diesel NO_x–PM tradeoff and support its viability as a low-emission CI fuel.

Keywords: dimethyl ether; compression ignition; exhaust gas recirculation; NO_x emissions; particulate matter; alternative fuels; diesel engines

1. Introduction

1.1. Background and Motivation

Diesel-fueled compression ignition engines have a tradeoff between NO_x and PM emissions [1]. Engine developers find an optimal point in this tradeoff and then specify an aftertreatment system to reduce the remaining emissions. Cooled exhaust gases recirculate back into the intake to dilute the air with inert gases of a higher specific heat. This results in lower combustion temperatures and less oxygen availability, reducing the formation of NO_x. In diesel-fueled engines, this reduction in combustion temperatures and dilution results in a greater formation of PM. DME is an alternative compression ignition fuel with a high cetane number (~55) that shows promise with high EGR tolerance and low NO_x/PM tradeoff [2]. The goal of this research is to determine the optimal operating conditions for low emissions and high efficiency of DME while maintaining diesel baseline brake power.

DME is gaining attention as a promising alternative fuel for CI engines due to its ability to significantly reduce emissions while maintaining performance [3–5]. DME inherently

Check for updates

Academic Editor: Roberto Finesso

Received: 19 January 2026
Revised: 16 April 2026
Accepted: 18 April 2026
Published: 19 May 2026

Copyright: © 2026 by the authors. Licensee MDPI, Basel, Switzerland. This article is an open access article distributed under the terms and conditions of the Creative Commons Attribution (CC BY) license.

produces very low PM, even at high EGR rates, making it especially attractive for meeting stringent off-road emissions standards such as U.S. EPA Tier 4 Final (0.02 g kWh^{-1} PM) and EU Stage V (0.015 g kWh^{-1} PM) [6,7]. A study by Kim et al. demonstrated that, at a fixed IMEP, DME generated negligible soot emissions compared to diesel and sustained stable combustion at EGR rates up to 45% [5]. These characteristics demonstrate that DME's inherently low soot combustion and favorable response to EGR provide a viable pathway for reducing NO_x without the accompanying increase in PM that typically constrains diesel engines, enabling simultaneous control of both pollutants in heavy-duty applications.

1.2. Research Gap and Contributions

Previous studies on DME as a fuel for CI engines have consistently demonstrated its potential to achieve low PM emissions and, under optimized conditions, reduced NO_x emissions [4,5,8]. DME's high cetane number (~55) and oxygen content contribute to its non-sooting combustion, leading to near-zero PM emissions even without advanced aftertreatment systems [2]. For instance, research on agricultural tractor engines fueled with DME reported ultra-low soot and PM emissions, highlighting DME's suitability for applications requiring stringent emission standards [4].

NO_x emissions studies have shown that while DME combustion can produce lower NO_x levels compared to conventional diesel, achieving optimal NO_x reduction requires careful calibration of injection strategies and EGR rates. For example, a study on a heavy-duty CI engine demonstrated that DME could meet current and future emissions standards with minimal exhaust gas aftertreatment when operating at an efficiency-optimal NO_x level of around 8 g kWh^{-1}. This was achieved by balancing injection phasing, injection pressure, and EGR variations [9]. However, excessively high EGR rates can lead to combustion instability and reduced engine performance, indicating the need for optimized EGR strategies [10].

Unlike previous DME studies, which typically evaluate EGR effects at a single operating condition, this work performs a full EGR sweep at one speed–load point and extends the analysis to two additional operating points using both nominal and 50% EGR [11–13]. This provides a broader multi-condition assessment of DME's EGR tolerance while maintaining IMEP matched to a diesel baseline. By combining injection timing sweeps with EGR sweeps, this work identifies cycle-controllable strategies that optimize combustion phasing, minimize NO_x emissions, and preserve brake power. This approach provides a comprehensive mapping of DME's operational envelope, addressing a critical gap in prior studies and offering practical insights for engine calibration and real-world implementation of DME as a low-emission alternative fuel.

1.3. Key Variables and Performance Metrics in Compression Ignition Engines

The combustion and emissions characteristics of CI engines are strongly influenced by several key variables, including fuel properties, air–fuel mixing, injection timing, and the application of EGR. These variables determine the spatial and temporal distribution of temperature, pressure, and equivalence ratio, which in turn govern the formation of major emissions such as NO_x and PM.

NO_x form predominantly in the near-stoichiometric burned gas regions, where local temperatures are highest and oxygen is sufficiently available for the thermal NO_x mechanisms to occur [1]. Conversely, soot, the main component of PM, forms within the fuel-rich zones of the spray core, where limited oxygen availability prevents complete oxidation of hydrocarbons. Within these regions, hydrocarbon fragments polymerize and nucleate into solid carbon particles.

The spatial distribution of air–fuel ratios thus determines the balance between NO_x and soot formation. Improved mixing reduces fuel-rich regions, promoting soot oxidation and decreasing PM emissions. However, enhanced mixing also increases local temperatures, which can elevate NO_x formation. This tradeoff, known as the soot–NO_x tradeoff, is a defining characteristic of diesel combustion [14]. Experimental results by Hountalas et al. demonstrated this behavior. Increasing EGR decreased NO_x emissions through charge dilution and lower flame temperatures but simultaneously increased soot due to inhibited oxidation [15].

CO and THC are direct indicators of incomplete combustion in compression ignition engines. They form when local temperatures or oxygen levels are too low for the oxidation reactions that convert CO to CO_2 and hydrocarbons to stable products. Heywood notes that low-temperature regions, spray impingement on chamber walls, and crevice volumes all provide environments where these reactions cannot fully proceed [1]. As a result, CO and THC typically originate in fuel-rich or overly diluted pockets that do not burn completely. Because they respond strongly to any condition that slows or weakens combustion, CO and THC are useful signals that the combustion process is no longer fully efficient.

The properties of the fuel play a fundamental role in defining engine behavior and emissions. Diesel fuel, the conventional CI fuel, is characterized by its cetane number, a measure of ignition quality analogous to the octane number in spark-ignition engines. The John Deere 6068CI550 engine used in this study operates on diesel fuel meeting ASTM D975 specifications for ultra-low-sulfur diesel (ULSD) [16]. According to ASTM D975, ULSD fuel of S15 grade must have a minimum cetane number of 40, while John Deere recommends at least 45, or 50 for cold or high-altitude conditions [17]. Diesel is liquid under ambient conditions, offering high energy density with a lower heating value (LHV) of approximately 42.6 MJ/kg [18].

DME, an alternative fuel, has emerged as a promising low-emission substitute for diesel. DME exists as a gas at ambient conditions but can be liquefied at pressures above 5.31 bar at 20 °C [2]. Its LHV is 28.9 MJ/kg, lower than diesel, requiring higher mass flow rates for equivalent energy delivery [18]. However, DME possesses a cetane number greater than 55, ensuring excellent ignition quality. Moreover, its molecular structure contains oxygen, which supports more complete combustion and virtually eliminates soot formation under typical diesel operating conditions [2]. The use of oxygenated fuels such as DME can therefore help decouple the soot–NO_x tradeoff by providing internal oxygen for soot oxidation even in fuel-rich regions. Zhu et al. demonstrated that increasing fuel oxygen content allowed NO_x to decrease with EGR addition while maintaining nearly constant soot emissions [19].

Injection timing is one of the most influential engine control parameters affecting both performance and emissions. Advancing injection timing allows combustion to occur earlier in the expansion stroke, increasing in-cylinder pressure and temperature, which improves efficiency but tends to increase NO_x emissions. Conversely, retarding injection timing delays combustion, reducing temperature and NO_x formation but often resulting in incomplete combustion and higher PM emissions. Raeie et al. observed that early injection timing in a CI diesel engine produced lower PM emissions but higher NO_x levels [20]. A separate study found that retarded injection timing reduced NO_x but increased soot due to incomplete oxidation in cooler, fuel-rich regions [21]. These results show the role of injection phasing in balancing the soot–NO_x tradeoff.

EGR is another key variable that affects both combustion and emissions. EGR involves redirecting a portion of the exhaust gases back into the intake air stream. This process introduces inert gases such as CO_2 and H_2O, which dilutes the air, reducing the percent of oxygen in the intake charge and increasing the specific heat capacity of the intake mixture,

lowering combustion temperatures and consequently reducing NO_x formation [1]. Beyond temperature effects, EGR alters combustion kinetics and stability. Higher EGR rates reduce the intake oxygen concentration and slow the overall reaction rate, extending ignition delay and retarding combustion phasing [22]. Although moderate EGR levels can reduce NO_x, excessive EGR may increase combustion instability and limit load capability. This instability is typically quantified by the COV of the IMEP and COV of CA50 [1,23]. High EGR can elevate the COV of the IMEP, especially at low loads, while moderate levels can enhance stability at higher loads [24,25].

The performance and emissions of CI engines depend on fuel properties, combustion phasing, and charge conditions. Higher temperatures and improved mixing increase efficiency but increase NO_x, while lower temperatures and oxygen-deficient regions promote soot formation. By adjusting fuel type, injection timing, and EGR rate, both NO_x and PM emissions can be reduced while maintaining comparable power output. This study evaluates the combustion, emissions, and performance of DME relative to diesel through parameter sweeps of injection timing and EGR at representative operating conditions.

2. Materials and Methods

2.1. Engine Test Cell and Controls

Testing for this research was conducted on a John Deere 6068CI550 diesel engine. The 6068CI550 is an industrial diesel engine designed to meet U.S Final Tier 4 emissions standards using split injection, EGR, and variable injection pressure. An image of this engine test cell and DME fuel system is shown in Figure 1, and some basic engine information is shown in Table 1.

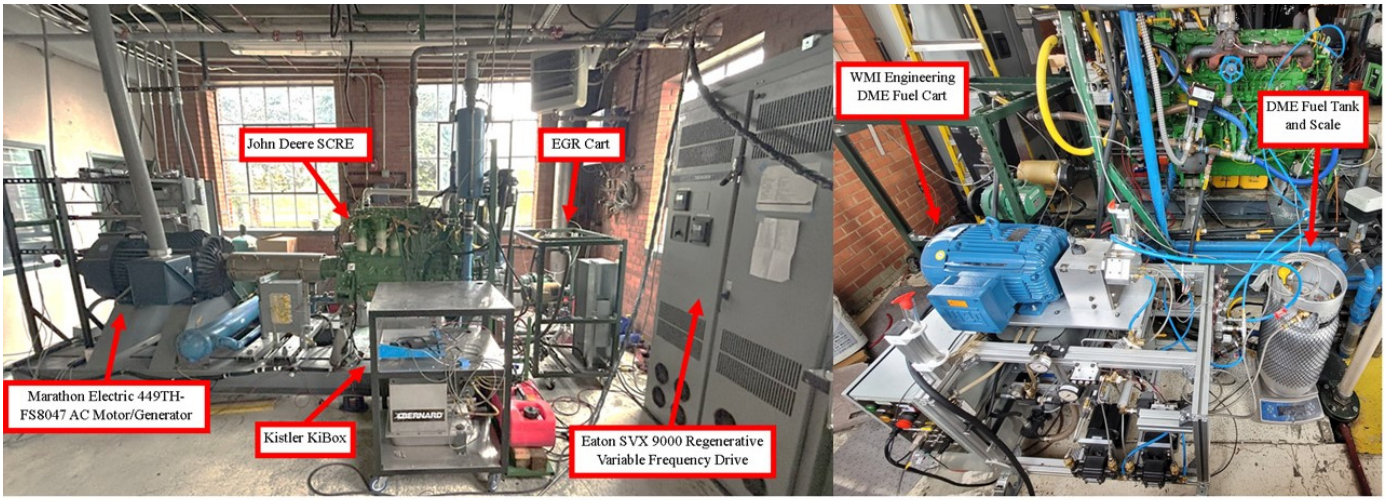

Figure 1. (**a**) John Deere 6068CI550 SCRE Test Cell (**b**) DME Fuel System and Scale.

For this study, the 6-cylinder engine was converted into an SCRE with a 1.12 L displacement, corresponding to about one-sixth of the total engine displacement. The engine is capable of operation up to 224 kW at 2400 rpm in the stock, 6-cylinder configuration.

The test cell shown in Figure 1 uses a Marathon Electric 449THFS8047 AC motor/generator coupled to an Eaton SVX 9000 regenerative variable-frequency drive (VFD). This system enables both motored operation and engine loading. The VFD provided closed-loop speed control, modulating the applied load to hold the engine at the commanded speed and supplying motoring power when combustion was absent.

Table 1. Key specifications of test cell engine.

Engine Name	John Deere 6068CI550
Engine Type	In-line, single cylinder, water cooled, four stroke
Bore	106 mm
Stroke	127 mm
Displacement	6.8 L
Compression Ratio	16.7:1
Rated Power	224 kW
Rated Speed	2400 rpm
Number of Valves	4
Fuel System	High-Pressure Common Rail
Electronic Control Unit	L33 Controller

The engine's air intake used compressed dry air from the facility's air supply. The intake pressure could be varied up to 60 psig. The compressed air passed through an intake heat-exchanger system to simulate turbocharger outlet temperatures. A Woodward throttle valve, controlled through the LabVIEW system, then regulated the compressed air pressure to the desired intake pressure. The system also included an exhaust backpressure valve (Woodward GloTech) to simulate the effects of the turbocharger's exhaust turbine. Finally, the EGR cart pumped exhaust gases into the intake manifold, controlling EGR temperature and flowrate. A summary of the test cell configuration, including controllers and instrumentation, is shown in Figure 2.

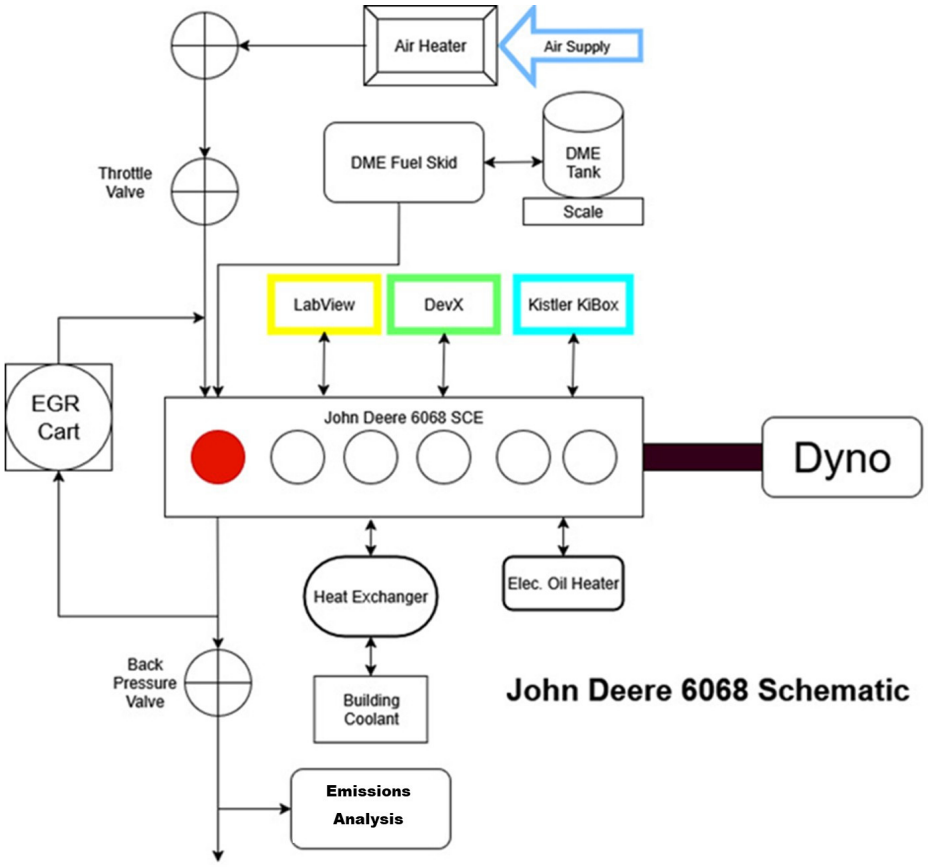

Figure 2. Test cell schematic in the DME configuration.

Two fuel system configurations were utilized depending on the test fuel. During diesel operation, a dedicated fuel skid equipped with a 6-gallon tank, lift pump, fuel cooler, and scale for fuel consumption measurement was used. The low-pressure circuit interfaced with the John Deere fuel system at the stock low-pressure pump above one of the fuel filters, and the return line routed fuel from the manifold back to the tank through the cooler. A John Deere RE549641 800 cc injector was used for all diesel testing.

For DME operation, DME supplied by Oberon Fuels meeting ASTM D7901 specifications was used [26]. A Flame King 33.5 lb propane cylinder served as the fuel reservoir and was mounted on a scale to determine mass flow. Low-pressure supply and return lines connected the tank to a DME fuel cart provided by WMI Engineering. The cart incorporated both low- and high-pressure pumps that operated in conjunction with the John Deere common-rail pressure regulator to maintain the desired rail pressure. A John Deere RE550611 1000 cc injector was installed for all DME testing to provide the higher mass flow rates required.

An EGR test cart was used to supply variable, conditioned exhaust flow. Originally developed for a CFR engine and then later adapted for a Cummins X15 SCRE [27], the cart was modified with a John Deere RE535729 EGR heat exchanger to meet the requirements of the 6068CI550 SCRE. Exhaust gases from the high-pressure exhaust manifold port enter the cart, where gas temperature (typically 350–550 °C) is reduced using the John Deere air–water heat exchanger. The desired EGR gas temperature was specified by the user, and a LabVIEW-controlled valve (Honeywell ML7425A3013) adjusted coolant flow to achieve this condition.

Engine and test cell operation were controlled through two primary modules, the John Deere L33 controller and a National Instruments (NI) PXI-1050 chassis equipped with 6224 and 6704 modules. The NI-based data acquisition and control system operated through a custom LabVIEW virtual instrument that regulated throttle position, intake air pressure and temperature, exhaust backpressure, EGR rate, and dynamometer speed. This system provided low-speed sampling for overall test cell control and monitoring, recording temperatures, pressures, and flow rates at 2 Hz.

The John Deere L33 controller was selected for this research because it enabled full control of the engine's fuel system. The L33 managed the Denso HP6 high pressure common-rail system used for diesel operation, including rail pressure regulation and single or multiple injection events per cylinder referenced to top dead center (TDC). The controller was compatible with multiple John Deere injector sizes and, being natively integrated with the test engine, provided a straightforward path toward potential DME fuel commercialization.

In-cylinder combustion was characterized using a Kistler KiBox system. The engine was instrumented with several Kistler in-cylinder pressure transducers and high-speed transducers on the intake and exhaust manifolds. These sensors provided crank angle-resolved pressure data for combustion analysis in cylinder one. A crankshaft encoder provided precise engine position and speed for signal synchronization. Using these inputs, the KiBox generated live pressure traces, apparent heat release, heat release rate, IMEP, peak pressure, peak pressure location, CA10–90, and CA50. Indicated power was computed from the in-cylinder pressure measurements and later converted to brake power using confidential mechanical efficiency data provided by John Deere. All pressure data were recorded at a resolution of 0.1 crank angle degrees.

2.2. Emissions Sampling

Emissions measurements were performed at both the intake and exhaust to quantify EGR rate, air–fuel ratio (AFR), and exhaust gas composition. Both intake and exhaust

samples were routed through heated sampling lines to a remote emissions analyzer located in the control room. Exhaust gas was sampled from a port downstream of the exhaust throttle, while intake gas was sampled from a port in the intake elbow upstream of the intake runners.

A Siemens 600 Series 5-Gas Analyzer measured CO, CO_2, NO_x, O_2, and THC. An MKS MultiGas 2030 FTIR spectrometer quantified formaldehyde, DME, diesel, and speciated hydrocarbons up to C_3, as well as NO and NO_2 concentrations.

PM samples were collected from the exhaust using a heated sampling line to prevent condensation and loss of semi-volatile material. The raw exhaust was diluted with conditioned building air to achieve a target dilution ratio appropriate for filter loading and to maintain temperatures suitable for PM collection. The diluted exhaust was then directed into a PM sampling cart equipped with a flow control system and a cyclone that removed larger particles and allowed collection of $PM_{2.5}$, defined as particles with an aerodynamic diameter of 2.5 μm or smaller. This ensured consistent sampling of fine particulate matter relevant to diesel and DME combustion.

PM was collected on a Teflon filter for gravimetric mass measurement and on a quartz fiber filter for carbon speciation. The PM collection and gravimetric analysis in this study were carried out following the procedures described by L'orange et al. (2021) [28]. Gravimetric filters were equilibrated to the balance environment and weighed to a resolution of one microgram. Each filter was weighed at least three times, and measurements were accepted once successive readings agreed within five micrograms. After sampling, filters were again equilibrated and reweighed using the same procedure. The difference between the pre sampling and post sampling masses was used to calculate the collected PM mass.

Quartz filters were analyzed for OC and EC using a Sunset OC/EC analyzer following the thermal optical protocol outlined in the NIOSH 5040 method [29]. The analyzer heats the sample in defined temperature steps under inert and oxidizing atmospheres and determines OC and EC fractions based on the optical correction point where pyrolyzed carbon returns to baseline. This analysis provided quantitative measurement of carbonaceous PM composition, complementing the gravimetric mass measurements and enabling detailed assessment of particulate emissions across the operating conditions tested.

2.3. EGR Rate Determination

The rate of EGR is defined as the percent of intake mixture that is recycled exhaust gas. This is calculated on a mass basis through the ratio of EGR mass in the intake to the that of the mass of fresh air and fuel. This can be seen in Equation (1) [1]:

$$EGR\ Rate\ (\%) = \left(\frac{m_{EGR}}{m_{Fuel} + m_{Air}} \right) \times 100 \quad (1)$$

where *EGR Rate* is the exhaust gas recirculation fraction expressed as a percentage (%), m_{EGR} is the mass flow rate of recirculated exhaust gas, and m_{Fuel} and m_{air} are the total inducted mass flow rates of fresh air and injected fuel, respectively. All mass flow rates are expressed in units of mass per time (e.g., kg/s).

The rate of EGR can also be determined from the ratio concentration of CO_2 in the exhaust and the concentration of the CO_2 in the intake. Hussain et al. (2012) [30] and Desantes et al. (2010) [31] both used this method to determine EGR rates in their studies. This can be seen in Equation (2):

$$EGR\ Rate\ (\%) = \left(\frac{[CO_2]_{int} - [CO_2]_{amb}}{[CO_2]_{exh} - [CO_2]_{amb}} \right) \times 100 \quad (2)$$

where $[CO_2]_{int}$ is the measured carbon dioxide concentration in the intake mixture, $[CO_2]_{exh}$ is the carbon dioxide concentration in the exhaust stream, and $[CO_2]_{amb}$ is the ambient atmospheric carbon dioxide concentration. CO_2 concentrations are reported on a volumetric basis by the gas analyzer (vol% or ppm), and must be expressed in consistent units when used in the EGR calculation.

A further simplification can be made by assuming that the CO_2 present in the atmosphere is negligible, which results in this simplification for EGR rate calculations by Zheng et al. 2004 [32]:

$$EGR\ Rate\ (\%) = \left(\frac{[CO_2]_{int}}{[CO_2]_{exh}} \right) \times 100 \quad (3)$$

The simplified EGR rate calculation seen in Equation (3) was used for EGR rate calculations in this study. The CO_2 concentrations were determined through emissions sampling ports on the intake and exhaust of the SCRE. The 5-gas emissions analyzer was used to determine the CO_2 concentration from these sampling ports.

2.4. Testing Procedure

A combination of the ISO 8178-4 C1 test cycle conditions and parameter sweeps was used for baseline diesel and DME testing.

For this study, only modes 2, 3, and 7 of the C1 cycle were selected to represent typical mid-load and high-load operating regions. These modes were chosen based on tractor engine operating data provided by John Deere. Engine load was determined using IMEP based on guidance from John Deere. A live 200-cycle average IMEP reported by the Kistler KiBox was used during testing. A summary of the test plan is shown in Table 2.

Table 2. Summary of Test Plan.

ISO 8178-4 C1 Test Cycle	Objective	Fuel	Engine Speed (rpm)	Load IMEP (bar)	EGR Rate (%)	Injection Timing (deg BTDC)	CA50 (deg ATDC)
Mode 2	Baseline	Diesel	2200	8.6	22	2.3	21
Mode 3	Baseline	Diesel	2200	6.84	24	5	20
Mode 7	Baseline	Diesel	1600	7.29	22	3.5	16
Mode 7	Injection Sweep	DME	1600	7.29	22	−1, 1, 3, 5, 6, 7, 9, 11, 13	16
Mode 7	EGR Sweep	DME	1600	7.29	22, 25, 30, 40, 50	Variable	16
Mode 2	Baseline Comparison	DME	2200	8.6	22	Variable	16, 21
Mode 2	Max EGR	DME	2200	8.6	50	Variable	16, 21
Mode 3	Baseline Comparison	DME	2200	6.84	24	Variable	16, 20
Mode 3	Max EGR	DME	2200	6.84	50	Variable	16, 20

At each test condition, key parameters such as exhaust pressure, intake temperature and pressure, coolant and oil temperatures, and EGR temperature were maintained at constant values, as summarized in Table 3.

Table 3. Constant Operating Conditions.

		Operating Condition		
Parameter	**Units**	**1600 rpm, 50% Load**	**2200 rpm, 50% Load**	**2200 rpm, 75% Load**
Exhaust Pressure	bar (a)	1.58	2.18	2.38
Intake Pressure	bar (a)	1.36	1.36	1.8
Intake Temperature	°C	50	50	55
Coolant Temperature	°C	99	99	99
Oil Temperature	°C	109	110	112
EGR Temperature	°C	104	110	117

In addition to the C1-cycle test points, parameter sweeps were conducted to characterize DME combustion behavior. Injection timing sweeps and EGR rate sweeps were performed while maintaining key operating parameters at constant values. Rail pressure was maintained at 135 MPa based on guidance from WMI Engineering. For both sweep types, IMEP was held constant by adjusting the injected fuel quantity per stroke. The resulting optimal CA50 from the injection timing sweeps was then held constant during the EGR sweeps. Additional boost was supplied at high EGR rates when increased fueling alone was insufficient to maintain IMEP.

2.5. SCRE Background and Approach

Several approaches exist for converting multi-cylinder engines to SCRE. One method isolates a single cylinder for experimentation while the remaining cylinders continue to drive the engine [33]. Other approaches achieve complete cylinder deactivation by either preventing compression through piston modifications or by removing the cylinder head entirely [34]. Alternatively, the valve train of the deactivated cylinders can be disabled so that a fixed mass of air remains trapped in the inactive cylinders [35].

For the conversion of the 6068CI550 to a SCRE, the chosen approach was to deactivate the valve train for cylinders two through six, creating a fixed trapped air volume in each of the non-firing cylinders. This method followed standard practice recommended by John Deere.

The conversion process required removal of numerous engine components, including the turbochargers and associated piping, EGR cooler, EGR valve, throttle, starter, alternator, and intake manifold. Several components were replaced or modified for single cylinder operation. The coolant manifold, cylinder head, exhaust manifold, intake system, and oil pan were all replaced with custom single-cylinder components. The injectors for cylinders two through six were disconnected to fully deactivate fuel delivery.

2.6. Cylinder Head

A custom cylinder head was designed and machined for converting the engine to an SCRE configuration. The head was machined at cylinder one to provide direct access to that cylinder's intake runner. The John Deere 6068CI550 uses a common plenum intake with cast runners integrated into the head, making machining necessary to isolate cylinder one for SCRE operation.

The glow plug ports on cylinders one and six were originally machined to accept liquid-cooled AVL QC34C pressure transducers for combustion pressure measurements. Due to availability constraints, adapters were later designed and machined to fit Kistler 6052C pressure transducers instead. Both transducers were mounted directly to the combustion chamber following Kistler's installation guidelines [36]. A second pressure transducer was added to cylinder one for redundancy. A Kistler 6052C transducer was installed through a cross-drilled passage machined into the head.

A custom intake elbow was fabricated, and modifications were made to the exhaust manifold to interface with the SCRE cylinder head. The intake elbow was modified with three ports to accommodate a K-type thermocouple, a Kistler Type 4007D dynamic pressure transducer, and an intake gas sampling line for lambda and EGR rate measurements. The exhaust manifold was also modified with additional ports and block-off plates at the deactivated cylinders, while retaining the original EGR and high-pressure turbo ports. Custom adapter plates were fabricated to mount a flow control valve for the external EGR system and to connect the exhaust manifold outlet to the test cell exhaust. The cylinder-one exhaust runner was machined to accept a liquid-cooled Kistler Type 4049B dynamic pressure transducer and a 3/16-inch K-type thermocouple.

2.7. Valve Train Deactivation

With the choice to use a trapped-air cylinder deactivation method, the valve train needed to be deactivated on the unused cylinders.

To deactivate the unused cylinders, the lifters, pushrods, rocker arms, and associated hardware were removed. To maintain proper oil pressure to the active cylinder-one valve train, custom rocker arm sleeves were designed and installed on the deactivated cylinders. The sleeves matched the spacing and tolerances of the OEM rocker arms, and one sleeve was used per deactivated cylinder, as seen in Figure 3.

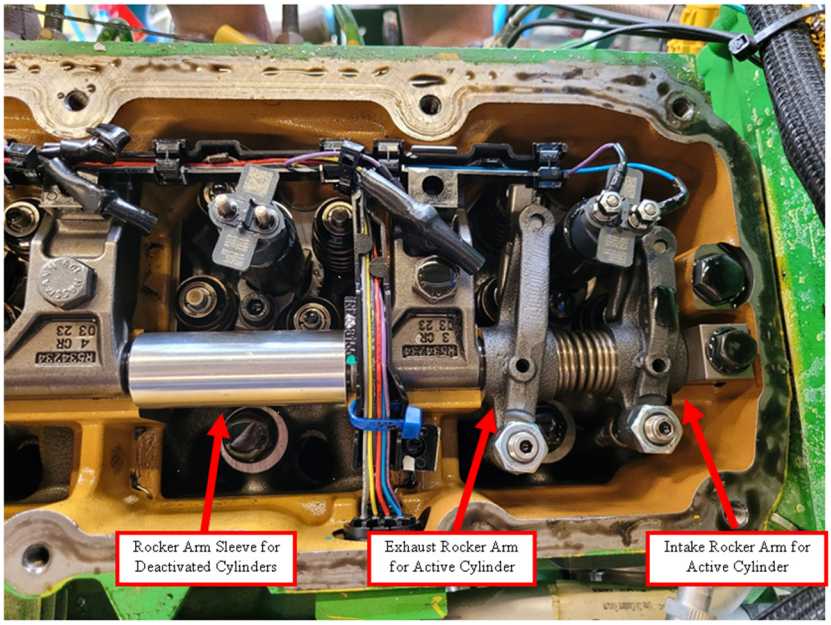

Figure 3. Valve train configuration with rocker arm spacers for cylinders #2-#6.

The unused cylinders were fully sealed from the intake and exhaust once the valve train components were removed. The valve train configuration of cylinder one remained unchanged and installation of the custom sleeves-maintained cylinder one oil pressure.

3. Results and Discussion

The baseline testing defines the initial performance condition of the SCRE on diesel and helps to compare it to the performance of the SCRE on DME. Modes 2, 3, and 7 from the ISO 8178-4 C1 test cycle were chosen as operating points for baseline testing. No parameter sweeps were conducted for baseline testing. Brake-specific emissions and combustion characterizations were used to baseline the diesel SCRE performance to compare to DME.

3.1. Combustion Parameters

Baseline diesel and DME combustion is shown in Figures 4 and 5 using cycle-averaged in-cylinder pressure and AHRR. The comparison evaluates combustion behavior across the three baseline operating points using a common set of parameters: SOI-CA5, CA50, CA10–90, peak pressure, the crank angle location of peak pressure, maximum AHRR, and location of maximum AHRR. Each condition was run according to the procedures outlined in Table 2, with injection quantity and timing fixed for diesel, and with CA50, EGR rate, and IMEP matched to the diesel baseline for DME. The resulting diesel combustion parameters are summarized in Table 4, and the corresponding DME results are presented in Table 5. Using identical metrics for both fuels provides a consistent basis for comparing

combustion phasing, heat release duration, and pressure development under matched operating conditions.

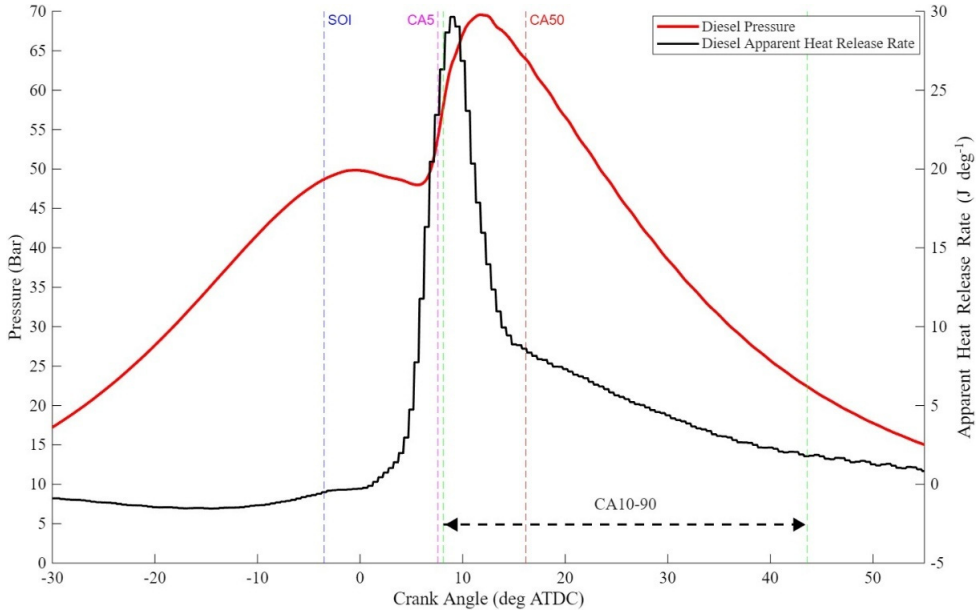

Figure 4. Diesel average pressure trace and apparent heat release rate at 1600 rpm and 50% load.

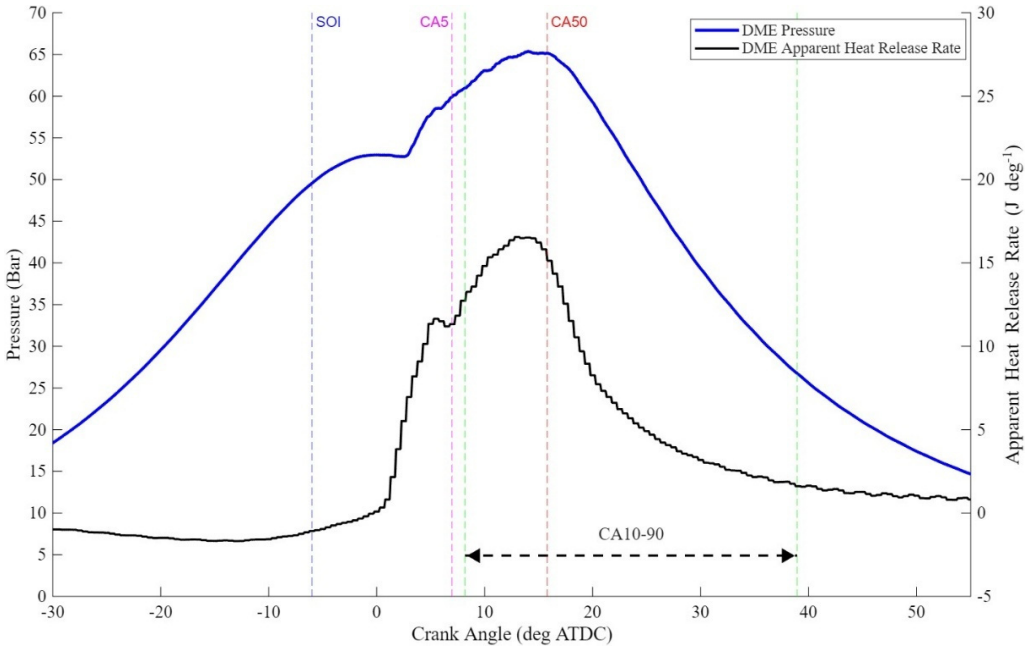

Figure 5. DME average pressure trace and apparent heat release rate at 1600 rpm and 50% load.

Table 4. Diesel Baseline Combustion Parameters.

		Diesel Operating Condition		
Parameter	**Units**	**1600 rpm, 50% Load**	**2200 rpm, 50% Load**	**2200 rpm, 75% Load**
SOI-CA5	deg	11.08	15.05	11.94
CA50	deg ATDC	16.17	19.96	20.80
CA10–90	deg	35.46	38.27	37.86
Peak Pressure	bar (a)	73.60	63.56	69.04

Table 4. *Cont.*

		Diesel Operating Condition		
Parameter	**Units**	**1600 rpm, 50% Load**	**2200 rpm, 50% Load**	**2200 rpm, 75% Load**
Location of Peak Pressure	deg ATDC	12.31	12.96	15.23
Peak AHRR	J deg^{-1}	29.65	23.21	19.40
Location Peak AHRR	deg ATDC	8.80	11.30	15.80

Table 5. DME Combustion Parameters.

		DME Operating Condition		
Parameter	**Units**	**1600 rpm, 50% Load**	**2200 rpm, 50% Load**	**2200 rpm, 75% Load**
SOI-CA5	deg	12.97	17.20	17.79
CA50	deg ATDC	15.79	20.05	20.37
CA10–90	deg	30.76	34.34	33.39
Peak Pressure	bar (a)	66.16	59.88	74.49
Location of Peak Pressure	deg ATDC	14.33	11.13	9.30
Peak AHRR	J deg^{-1}	16.55	13.29	14.89
Location Peak AHRR	deg ATDC	12.80	19.80	20.80

All in-cylinder pressure traces and AHRR plots presented in this study represent cycle-averaged combustion data computed from 1600 consecutive engine cycles at each operating condition. This cycle count was selected to ensure stable averaging and consistent comparison between fuels. The AHRR traces exhibit some noise in the signal. To mitigate this effect while preserving the shape and timing of the heat release features, a moving average smoothing window of 5 points was applied to all AHRR curves.

Figure 4 shows diesel combustion at 1600 rpm and 50% load. The AHRR trace shows two main stages of diesel combustion. The initial sharp spike in heat release immediately after ignition corresponds to the premixed phase, where fuel that accumulated during the ignition delay burns very rapidly. This is followed by a longer, gradual decline in AHRR that reflects the diffusion-controlled phase, during which fuel continues to burn as it mixes with air. Phasing markers for SOI, CA5, CA50, and CA10–90 identify the key stages of combustion.

Figure 5 presents DME combustion at 1600 rpm and 50% load. The AHRR trace for DME displays a broad and low-magnitude heat release profile. The absence of a sharp initial spike indicates that only a small fraction of the fuel accumulates prior to ignition. This produces a smoother rise in cylinder pressure and a reduced pressure rise rate compared to diesel, even though CA50 is matched between the fuels.

From the AHRR profiles, diesel consistently produces premixed heat release spikes that are approximately 50–75% larger than those of DME. This finding corresponds closely to diesel combustion theory, which attributes the magnitude of the premixed spike to the formation of partially vaporized, fuel-rich pockets that burn rapidly at the onset of high-temperature ignition [5,37]. The results measured here therefore reflect mechanisms described in Heywood 1988, where even with a shorter SOI–CA5 interval, diesel accumulates a substantial amount of reactive mixture before the start of combustion, producing a sharp heat release spike once ignition begins [1]. DME, by contrast, exhibits the broad, single-stage AHRR, which several authors have linked to its complete vaporization, highly uniform mixing, and lack of diffusion burning zones [3,37,38].

The combustion parameter results from diesel and DME baseline testing are presented in Tables 4 and 5, respectively. Across all conditions, DME operated with a consistently

shorter combustion duration than diesel, as indicated by lower CA10–90 values. SOI–CA5 also differed between the fuels, with DME exhibiting longer SOI–CA5, reflecting later start of combustion relative to injection. Peak pressure trends varied with operating condition. At 1600 rpm and 2200 rpm under 50% load, DME produced lower peak pressures than diesel, while at 2200 rpm and 75% load, DME reached a higher peak pressure. The location of peak pressure showed similar variation. At 1600 rpm and 50% load, DME's peak pressure occurred about 2 deg ATDC later than diesel; at 2200 rpm and 50% load, DME peaked roughly 2 deg ATDC earlier; and at 2200 rpm and 75% load, DME's peak pressure occurred substantially earlier, by approximately 6 deg ATDC. Maximum AHRR values were lower for DME at all shared operating conditions, consistent with its broader and more gradual heat release profile. The crank angle location of the maximum AHRR occurred later for DME at 1600 rpm, but earlier at the two 2200 rpm points, with the largest shift at 2200 rpm and 75% load, where the DME heat release peak occurred more than 5 deg ATDC ahead of the diesel case.

The SOI–CA5 results show that diesel consistently reaches 5% mass fraction burned sooner after SOI than DME. While DME is often noted for its short chemical ignition delay due to its high cetane number, several experimental studies have reported that pressure-based detection of ignition can appear later for DME in moderate load operation because its fast vaporization, high latent heat, and low early heat release intensity delay the onset of detectable HRR rise [3,5,37]. The longer SOI–CA5 values measured for DME in this work align with the literature and the observations that the timing of measurable heat release does not necessarily reflect the chemical ignition delay for DME and can be influenced by the weaker initial HRR signal.

The CA10–90 results also show strong agreement with the literature. Across all baseline points, DME burns over a narrower crank angle interval, with 4–5 deg shorter CA10–90 values than diesel. This reduction closely matches the 10–15% shorter burn durations reported by Stepanenko et al. 2019 [3], Kim et al. 2007 [5] and Arcoumanis et al. 2008 [37], who attribute this behavior to DME's rapid vaporization, enhanced premixing, and the absence of a diffusion-limited burn phase. In contrast, diesel's longer CA10–90 duration observed here is consistent with the persistent mixing-controlled combustion described by Heywood 1988 [1].

Peak pressure phasing also aligns with previously observed DME trends. In the present work, DME exhibits earlier peak pressure timing at higher speed and load but slightly later phasing at 1600 rpm and 50% load. Similar behavior was noted by Kim et al. (2007) [5] and Youn et al. (2022) [10], who reported that DME's phasing shifts depend strongly on charge temperature and mixing intensity. At higher speeds, faster mixing and more complete vapor phase distribution can advance combustion phasing, while at lower speeds, weaker early heat release can delay peak pressure location.

3.2. Emissions and Efficiency Comparisons

Emissions and efficiency comparisons for diesel and DME are presented in Table 6. The fuels are evaluated using brake-specific emissions of NO_x, and PM, as well as brake-specific fuel consumption and thermal efficiency. These metrics provide a direct, side-by-side assessment of fuel performance under matched combustion phasing conditions, where CA50, EGR rate, and IMEP are held constant between diesel and DME. Differences in mixing and heat-release structure between fuels are evaluated here using AHRR, combustion duration, and phasing metrics rather than direct temperature measurements.

Table 6. Summary of Emissions at Operating Conditions.

		Operating Condition					
		1600 rpm, 50% Load		2200 rpm, 50% Load		2200 rpm, 75% Load	
Parameter	**Units**	**Diesel**	**DME**	**Diesel**	**DME**	**Diesel**	**DME**
Brake-specific NO_x	g kWh^{-1}	0.80	0.45	0.49	0.40	0.59	0.35
Brake-specific PM	g kWh^{-1}	0.500616	0.136364	0.351734	0.183528	0.672431	0.238634
Brake-specific CO	g kWh^{-1}	2.97	0.67	8.37	3.43	3.37	2.06
Brake-specific THC	g kWh^{-1}	0.25	0.06	0.52	0.19	0.28	0.14
Brake-specific Fuel Consumption	g kWh^{-1}	258.27	371.54	337.01	523.62	260.15	436.74
Thermal Efficiency	%	32.95	33.53	25.13	23.79	32.50	28.52

Brake-specific nitrogen oxides ($BSNO_x$) emissions under matched CA50 and EGR rates show that DME produces lower NO_x than diesel, with the largest difference at 2200 rpm and 50% load, where diesel generates the highest NO_x level in the baseline set. This indicates that diesel sustains higher local peak temperatures during mixing-controlled combustion, whereas DME's rapid vaporization and oxygenated chemistry reduce peak temperature residence time and suppress thermal NO_x formation in this regime. Direct in-cylinder temperature measurements or modeled temperature fields were not available in this study, so temperature-related interpretations are based on established combustion theory and measured heat-release and emissions trends rather than direct temperature diagnostics. The opposite NO_x response with increasing load at 2200 rpm reflects diesel's diffusion-influenced heat release creating stronger localized high-temperature zones at higher fueling, whereas DME's fast vaporization and lack of diffusion-flame combustion produce a more spatially uniform burn that reduces hot-spot temperature residence time and therefore NO_x.

Brake-specific particulate matter (BSPM) emissions for DME demonstrate a dramatic reduction in PM across all operating conditions, aligning with its lack of C–C bonds and near-soot-free combustion properties. Although PM increases with load for both fuels, the increase is far less pronounced for DME, suggesting that load-driven enrichment plays a minimal role in particulate formation when fuel-bound oxygen is present. The increase in DME PM with engine speed does not follow typical diesel soot-oxidation behavior because DME particulate mass is dominated by organic carbon rather than soot, so it is governed more by incomplete oxidation and condensable organics than by soot burnout time. This behavior is consistent with the findings of Yanju et al., where the premise of the study was that DME PM originates from lubricant oil [39].

Figure 6 further resolves DME particulate emissions into OC and EC fractions. More than 95% of measured PM mass for all operating conditions is OC, indicating that emissions are dominated by volatile hydrocarbons rather than soot. This confirms that particulate formation is governed by fuel and oil vaporization rather than accumulation of carbon-based particulate matter commonly formed in diesel combustion. A comparable diesel reference study reported PM compositions with significant EC, as also shown in Figure 6 [40]. This study was looking at the PM composition for a 4-cylinder John Deere 4045 Tier 3 CI engine operating at Mode 4 of ISO 8178 (50% torque at 1700 rpm). This engine and operating point closely align with those used in this study, providing relevant insight into diesel PM composition. Nearly half of the PM mass from ULSD consists of EC, indicating a high proportion of soot. In contrast, DME PM contained less than 5% EC [40]. This stark difference demonstrates that diesel PM is predominantly soot-based, whereas DME produces minimal soot even under comparable conditions.

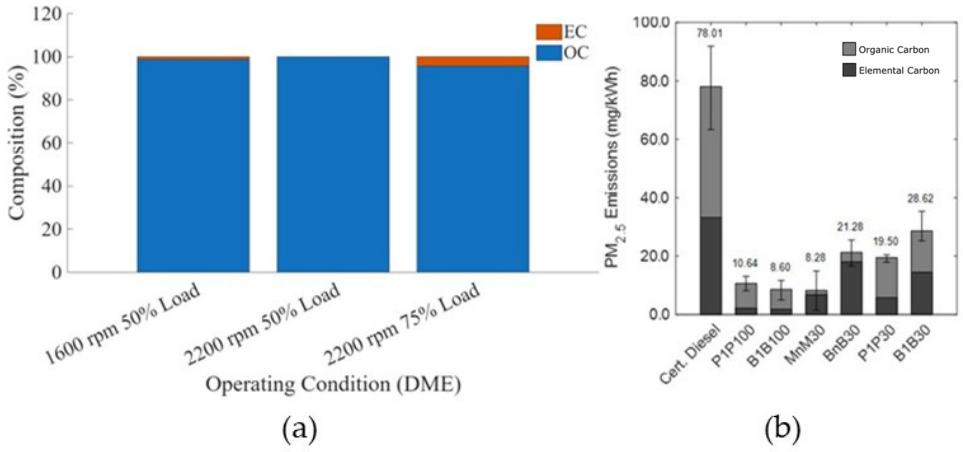

Figure 6. (**a**) Composition of DME brake-specific particulate matter emissions between organic (OC) and elemental carbon (EC). (**b**) Diesel brake-specific particulate matter emissions between organic and elemental carbon [40].

The BSFC results listed in Table 6 show that DME requires higher mass-based fuel flow due to its lower LHV. Despite this increase, the BSFC trend for DME closely mirrors that of diesel, with both fuels peaking at 2200 rpm and 50% load. This demonstrates that the primary driver of BSFC differences is fuel energy density rather than combustion efficiency.

At 1600 rpm and 50% load, diesel and DME operate at nearly identical thermal efficiencies. At the higher-speed conditions, diesel shows a slight efficiency advantage. Overall, the similarity in efficiency confirms that DME can operate with diesel-equivalent combustion phasing without significant thermal efficiency penalty.

Table 7 summarizes the measurement uncertainty for the key operating and emissions parameters used in testing. The table is based on a repeated test point at 1600 rpm, 50% load, and 22% EGR that was performed at the beginning of each test day. For each parameter, the variation was evaluated, and the uncertainty is reported as one sigma expressed as a percentage of the mean value. This focuses on repeatability from day to day for the complete experimental system rather than on the variability within a single run.

Table 7. Repeatability-Based One-Sigma Uncertainties for Engine Operating and Emissions Parameters.

Parameter	Unit	Uncertainty (%)
Engine Speed	rpm	±0.25
Intake Pressure	bar (a)	±1.17
Intake Temperature	°C	±6.58
Exhaust Pressure	bar (a)	±1.03
EGR Rate	%	±3.85
IMEP	bar	±2.99
CA50	deg ATDC	±1.97
Thermal Efficiency	%	±1.04
BSCO	g kWh^{-1}	±15.29
BSTHC	g kWh^{-1}	±22.44
BSNO$_x$	g kWh^{-1}	±8.93
BSPM	g kWh^{-1}	±6.03

The table shows that the engine operating conditions were very well controlled. Engine speed had the lowest uncertainty at ±0.25%, indicating that the dynamometer and control

system held the target speed accurately. Intake and exhaust pressures and IMEP remained within roughly ±1% and ±3%, respectively. CA50 uncertainty was ±1.97%, which is acceptable for combustion phasing measurements [1]. EGR rate uncertainty was ±3.85%, which reflects the sensitivity of the dilution level to small changes in pressure and flow but still indicates good control of the target operating condition. Brake thermal efficiency also showed a low uncertainty of ±1.04%, which shows that the overall energy balance of the engine and dynamometer system was stable from day to day.

The emissions measurements exhibited larger percentage uncertainties, which is expected when working with low engine-out emissions [41,42]. BSNO$_x$ uncertainty was ±8.93%, and BSPM was ±6.03%. The largest uncertainties occurred for BSCO and BSTHC at ±15.29% and ±22.44%, respectively. These higher values arise because the absolute concentrations of CO and THC for DME are very small, so even modest analyzer drift or noise appears as a large percentage difference.

The particulate matter behavior observed in this study is consistent with established trends for diesel and DME combustion. Diesel PM measured here increased with load but did not show a consistent dependence on engine speed. Although diesel OC/EC fractions were not measured directly, the diesel reference study by Windom et al. (n.d.) [40] shows that nearly half of diesel PM mass at similar load and speed conditions consists of EC. In contrast, DME PM increased with both load and speed in this study, but the absolute PM mass remained significantly lower than diesel across all baseline points. The OC/EC analysis performed on DME samples showed that more than 95% of particulate mass consisted of OC, with EC contributing less than 5% at every condition. This result is consistent with previous DME combustion studies. Kim et al. (2007) [5] reported nearly soot-free DME combustion due to rapid vaporization and minimized fuel-rich regions, while Zhang et al. (2008) [8] showed that DME PM levels are typically one to two orders of magnitude lower than those of diesel and that the PM mainly consists of volatile organic material consistent with OC.

The NO$_x$ trends observed in this study are consistent with previously reported DME behavior under comparable moderate EGR conditions. At the baseline EGR level of approximately 22–24%, DME produces roughly 10–35% lower brake-specific NO$_x$ than diesel. Similar reductions have been documented by Kim et al. (2007) [5], who found that DME consistently yields lower $_{NOx}$ than diesel at EGR levels representative of typical diesel operation. Studies by Arcoumanis et al. 2008 [37] and Putrasari et al. 2021 [38] report that DME's more homogeneous temperature field, lower peak temperatures, and reduced high-temperature residence time contribute to NO$_x$ suppression even under modest dilution, whereas diesel continues to exhibit the characteristic NO$_x$–soot tradeoff at similar EGR levels. These mechanism explanations are based on measured heat-release behavior and emissions trends and are interpreted as combustion-physics inference rather than direct temperature measurement.

Both fuels operated at comparable mixture strengths under all baseline conditions. At the matched operating points (1600 rpm 50% load, 2200 rpm 50% load, and 2200 rpm 75% load), diesel lambda values were 1.41, 1.37, and 1.47, while DME lambda values were 1.47, 1.48, and 1.49, respectively. Both fuels exhibited similar lambda values, indicating that the global equivalence ratio was effectively matched across operating points. Therefore, the lower NO$_x$ and PM observed for DME are attributed to the inherent chemical and physical properties of the fuel rather than to variations in global lambda.

The fuel consumption and thermal efficiency trends measured in this study are also in strong agreement with the broader body of DME research. Because DME's LHV is approximately two-thirds that of diesel on a mass basis, the higher brake-specific fuel consumption observed here is expected and reflects the differences in fuel energy density

rather than differences in combustion completeness. Despite this higher BSFC, the thermal efficiency of DME remains comparable to that of diesel across all baseline points. This behavior mirrors the findings of Arcoumanis et al. 2008, who reported that engines operating on DME frequently achieve similar or slightly improved indicated and brake thermal efficiencies, even while consuming a greater mass of fuel [37]. Similar trends were observed by Putrasari et al. (2021) [38] and Kim et al. (2007) [5], who attributed DME's efficiency to faster heat release rates, earlier combustion phasing, and reduced spatial and temporal temperature gradients, all of which contribute to lower heat transfer losses relative to diesel. Youn et al. 2022 [10] likewise demonstrated that DME maintains strong thermal efficiency across a wide operating range, despite requiring higher mass flow to achieve matched load. The alignment between these published results and those observed show that DME's higher BSFC does not carry an efficiency penalty and is primarily a reflection of fuel chemistry rather than a limitation of combustion performance.

Taken together, the baseline combustion, emissions, and fuel consumption results are in agreement with the DME combustion literature. Differences between diesel and DME in SOI–CA5 timing, combustion duration, peak AHRR, and PM composition match the mechanisms attributed in previous studies to fuel vaporization, mixture stratification, chemical kinetics, and the suppression of diffusion burning. The emissions and efficiency results further show that DME can achieve low NO_x and PM compared to diesel without penalties in CO or THC at comparable operating points. The uncertainty analysis in Table 7 strengthens this conclusion by demonstrating that key operating and performance parameters were well controlled and repeatable across days, with low one-sigma uncertainties for engine speed, pressures, IMEP, CA50, EGR, and brake thermal efficiency. Although the emissions measurements exhibited higher relative uncertainties, this behavior is expected at very low engine-out emission levels and does not affect differences observed between fuels. The alignment between the present experimental data and prior DME research reinforces the validity of the baseline comparisons used as the foundation for the combustion parameter sweeps, and the measured uncertainties further support the reliability of these conclusions.

The baseline comparison demonstrated that DME can operate at combustion phasing and thermal efficiency comparable to diesel, with reduced PM and NO_x emissions. Building on these results, a series of operating parameter sweeps were performed to evaluate how DME responds to injection timing and EGR dilution; NO_x tradeoff plots (e.g., CO vs. NO_x) are used as a means for performance evaluation. The purpose of this section is to characterize the sensitivity of DME combustion to these parameters and identify operating zones that achieve minimum emissions while maintaining acceptable fuel consumption.

3.3. Injection Timing Sweep

An injection timing sweep was conducted at 1600 rpm and 50% load to determine the combustion phasing sensitivity of DME relative to $BSNO_x$ and BSFC. IMEP and EGR rates were fixed for the sweep. The results are shown in Figures 7 and 8, where in-cylinder pressure traces and AHRRs are shown, and injection timing is expressed in terms of CA50 to unify the comparison across firing conditions.

Figure 7 presents the averaged in-cylinder pressure traces for the DME injection timing sweep conducted at 1600 rpm and 50% load. The figure shows the pressure evolution for injection timings ranging from 13 deg BTDC to 1 deg ATDC. All conditions follow a similar compression trajectory prior to ignition, after which the traces diverge according to the injection timing. Earlier injections produce higher peak pressures and an earlier rise in pressure relative to TDC, while later injections delay the start of combustion and lower the pressure rise rate.

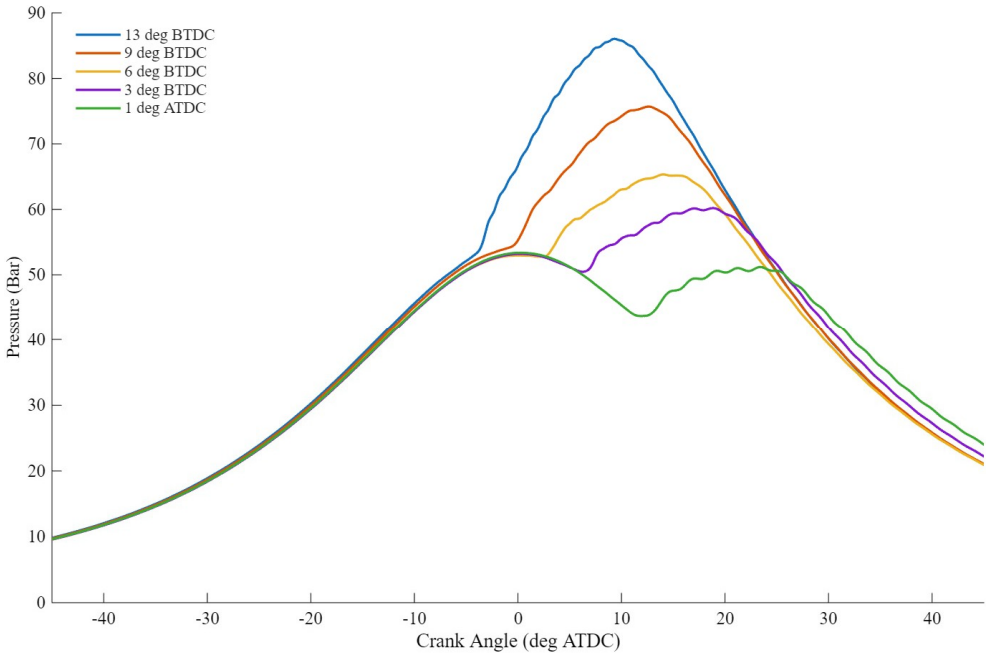

Figure 7. Average pressure traces for injection timing sweep at 1600 rpm and 50% load.

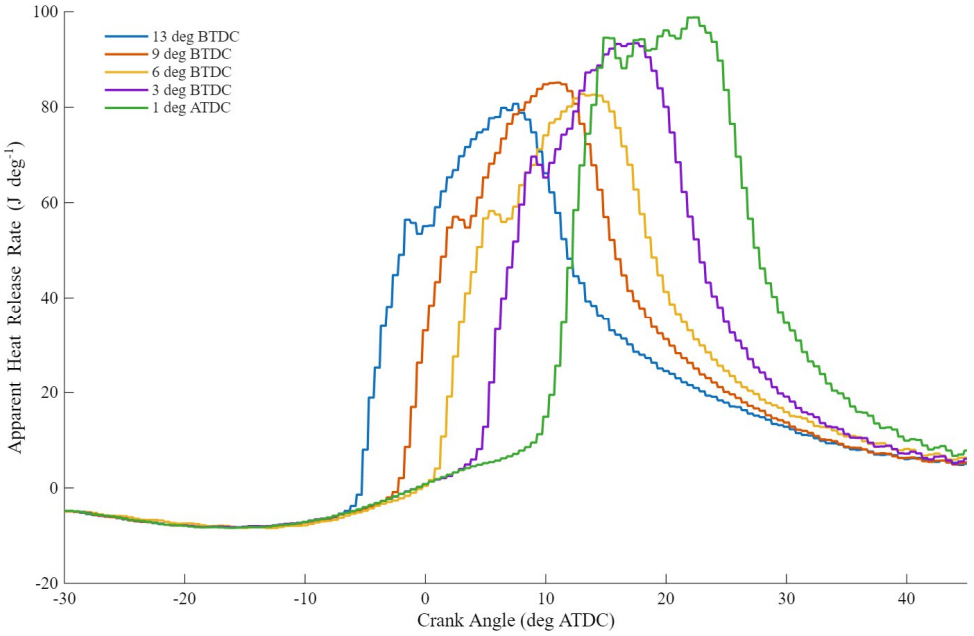

Figure 8. Apparent heat release rates for injection timing sweep at 1600 rpm and 50% load.

Figure 8 presents the AHRR for DME at 1600 rpm and 50% load across an injection timing sweep, showing how combustion phasing shifts as SOI is advanced or retarded. The most advanced case (13 deg BTDC) exhibits the earliest rise in heat release and an early, narrow main heat release peak. As injection timing is progressively retarded, the start of combustion moves later in the cycle, and the main heat release peak shifts accordingly toward more positive crank angles, with the curves becoming slightly broader and less sharply peaked. The most retarded case (1 deg ATDC) shows the latest onset of combustion and the most delayed peak heat release location, accompanied by a wider main combustion region.

The injection timing sweep results are interpreted using three linked indicators: heat-release structure, ignition-delay metrics, and combustion stability parameters. The pressure and AHRR traces in this study show a single premixed-type profile heat release across

all injection timings, consistent with the behavior reported by Kim et al. (2007) [5] and Arcoumanis et al. (2008) [37], who observed that DME in CI engines tends to burn in a broad, single-stage premixed fashion due to its high cetane number, high volatility, and lack of soot-forming C–C bonds. Similar single-stage premixed heat-release structures with reduced diffusion burning and reduced smoke have been observed for DME by Song et al. (2004) [43] and Huang et al. (1999) [44], who showed that homogeneous premixed combustion dominates and suppresses late diffusion flames. Roh et al. (2018) [45] and Park et al. (2012) [46] further showed that DME in a common-rail CI engine exhibits relatively smooth, premix-dominated AHRR profiles over a wide range of injection strategies, supporting the trends observed here. Together, these studies reinforce that the single-stage premixed heat-release patterns observed across the injection timing sweep are characteristic of DME combustion.

The relationship between CA50 and SOI–CA5, often referred to as ignition delay, showed that as CA50 moves later in the cycle, corresponding to progressively retarded injection timing, the SOI–CA5 duration generally becomes shorter, indicating a reduced delay between injection and the onset of combustion. SOI–CA5 steadily decreased from 13.38 deg to 12.39 deg until CA50 approached about 23 deg ATDC, which corresponds to the most retarded injection timing case (1 deg ATDC). At this point, the SOI–CA5 value levels off relative to earlier points at 12.90 deg.

The relationship between CA50 and CA10–90, which can be considered the combustion duration for the DME injection timing sweep at 1600 rpm and 50% load, showed how the main combustion duration changes as injection timing is retarded. As CA50 moves later in the cycle with progressively retarded injection timing, CA10–90 consistently decreases, indicating that the main combustion duration becomes shorter as timing is delayed. This trend persists across the full range of phasing, with the longest duration of 34.43 deg and shortest durations of 24.12 deg occurring at the most retarded conditions.

The SOI–CA5 interval shortens as injection timing is retarded because the charge temperature is higher near TDC and DME's ignition delay becomes very short under these warm conditions. Youn et al. 2022 reported that, in a DME-fueled CI engine, ignition delay is governed strongly by in-cylinder temperature and early reaction rates, rather than by the crank angle separation between injection and ignition [10]. Teng et al. 2003 also showed that DME's physical and chemical delays collapse rapidly once local gas temperature exceeds a critical level, making ignition timing highly sensitive to temperature and less dependent on injection timing in warmed conditions [47]. Spray ignition experiments by Cung et al. 2021 similarly demonstrated that DME autoignition occurs quickly once the vaporizing jet encounters sufficiently hot ambient gas, with shorter ignition delay and lower lift-off length than diesel under the same conditions [48]. This supports the observed SOI–CA5 trend, which decreases as in-cylinder temperatures rise due to the proximity to TDC.

CA10–90 follows the same trend. As timing is retarded, the CA10–90 burn duration decreases, reflecting a more compact and rapid release of heat within a narrower crank angle window. This observation aligns with studies on DME CI combustion by Huang et al. 1999, who reported that DME exhibits shorter combustion duration and more compact heat release when mixture preparation is favorable and in-cylinder temperatures are high, even when the peak heat release magnitude is reduced [44].

The COVs for IMEP and CA50 are generally indicative of combustion stability. Looking at the COVs of these parameters across the DME injection timing sweep at 1600 rpm and 50% load, it was observed that as CA50 shifts later with progressively retarded injection timing, the COV of CA50 steadily decreases, indicating improved cycle-to-cycle phasing consistency at more retarded timings. In contrast, the COV of IMEP remains generally uniform across the sweep, showing only modest variation with timing. A single outlier

appears near CA50 of about 13 deg ATDC, where the IMEP COV increases noticeably relative to the surrounding points.

Combustion stability metrics reveal additional insights. Across the timing sweep, the COV of IMEP remained below accepted stability limits for CI engines, which generally define stable operation as a COV of IMEP of less than about 5% [1]. In this sweep, the COV of IMEP stayed under 3.2%, indicating consistently stable combustion. The COV of CA50 decreases steadily as combustion is retarded, demonstrating that more consistent combustion phasing occurs when ignition takes place closer to the higher and more uniform cylinder temperatures near TDC. COV of CA50 values below 2–3% indicated stable phasing, and in this sweep, all conditions remained under about 2.5% COV of CA50 [1,49]. A DME cyclic variation study by Sezer 2025 showed that the COVs of CA50 and IMEP remain very low until combustion phasing is pushed to the edge of stable operation, at which point both metrics rise sharply as partial burn and misfire cycles appear [23]. This behavior is consistent with the trends observed in the present study, where COV values remain low throughout the timing sweep.

As injection timing is retarded across the sweep, the main combustion event shifts later into the expansion stroke, lowering peak temperature and residence time, which in turn suppresses NO_x formation and reduces overall heat release magnitude, although at the expense of fuel consumption. Earlier combustion phasing produces higher peak pressures and sharper heat release peaks due to elevated temperatures near TDC. NO_x levels do not fall below the diesel baseline until combustion is shifted to a CA50 of roughly 15 deg ATDC or later. These conditions increase thermal NO_x formation through the extended Zeldovich mechanism, which dominates NO_x production in conventional and moderately premixed CI operation [1,49].

Figure 9 shows the relationship between combustion phasing, NO_x emissions, and BSFC. As CA50 shifts earlier in the cycle, brake-specific NO_x increases and as CA50 is retarded, NO_x decreases steadily, and all data points with CA50 greater than approximately 15 deg ATDC fall below the diesel baseline NO_x level indicated by the dashed red line. BSFC displays an opposite trend where earlier CA50 points show lower BSFC values, while BSFC increases gradually as CA50 is retarded. The cluster of data points near a CA50 of 16 deg ATDC are additional daily points taken at the same operating conditions on each test day.

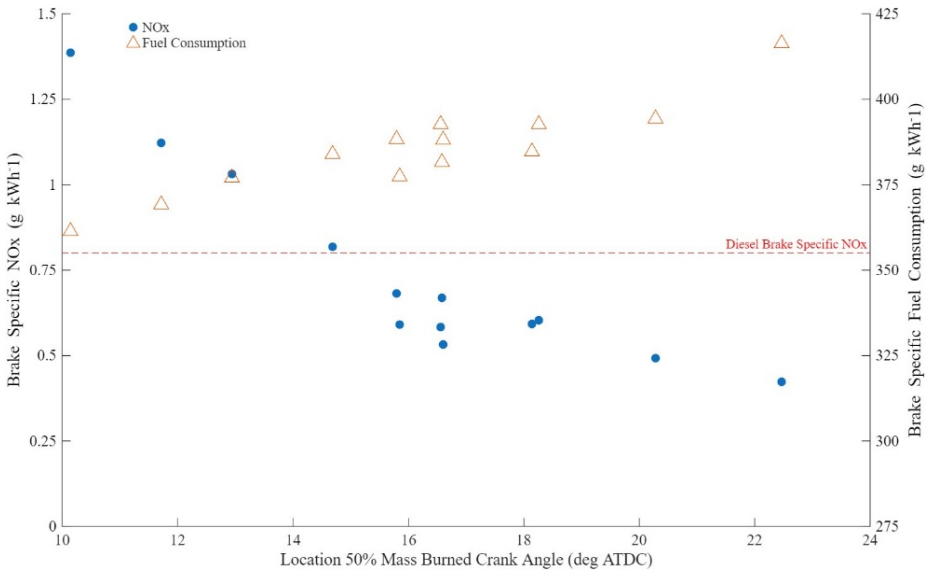

Figure 9. Location 50% mass burned crank angle vs. brake-specific nitrogen oxides and brake-specific fuel consumption.

When the combustion behavior is compared with emissions and fuel consumption trends, an optimal phasing becomes clear. Earlier phasing increases NO_x sharply, whereas late phasing degrades efficiency as combustion moves further into expansion. The point where NO_x is reduced without incurring a significant BSFC penalty corresponds to a CA50 of approximately 16 deg ATDC. This phasing is consistent with other DME CI studies that identified moderately retarded combustion phasing as the region that minimizes NO_x while preserving efficiency, particularly when combined with suitable EGR levels [10,37,50]. Zhang et al. 2009 reported that moving CA50 moderately into the expansion stroke reduces NO_x without a large efficiency penalty, while further retardation produces rising BSFC and incomplete combustion [51]. The injection timing sweep in this section therefore establishes an optimal CA50 at 16 deg ATDC for low NO_x and low PM DME operation.

3.4. EGR Sweeps

An EGR sweep was performed at 1600 rpm and 50% load to evaluate the effect of increasing dilution on NO_x reduction, the associated tradeoffs with other emissions, and the limits of combustion stability. For this sweep, IMEP and CA50 were held constant while EGR rate was varied. The resulting combustion and emissions behavior is presented in Figures 10–13, including in-cylinder pressure traces, AHRR, relationships between EGR rate and SOI–CA5 and CA10–90, COV for IMEP and CA50, and the corresponding emissions trends.

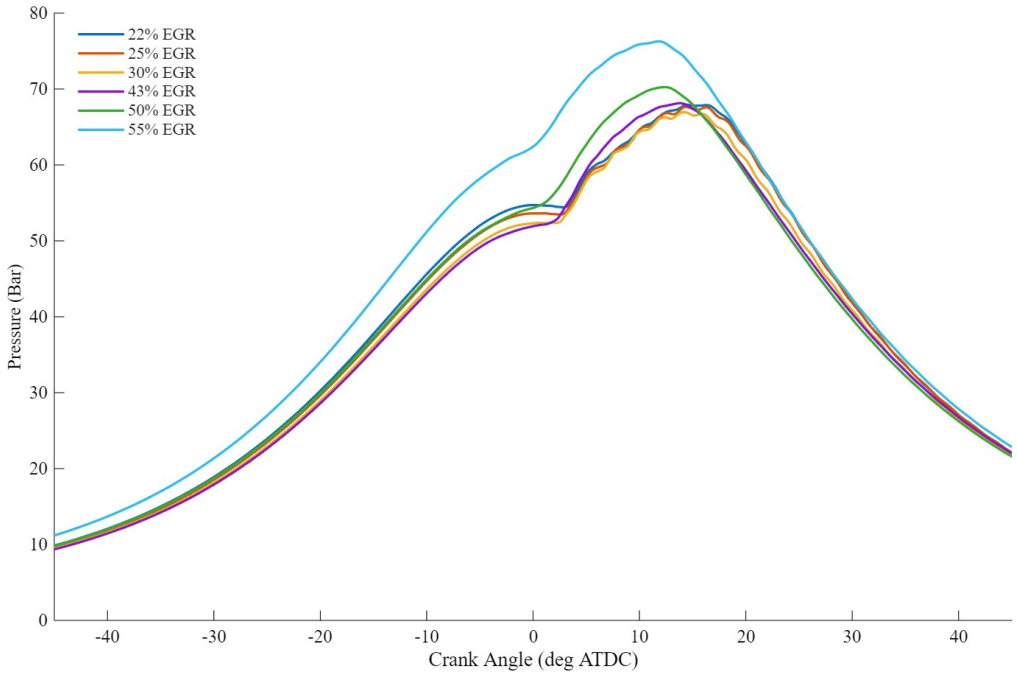

Figure 10. Average pressure traces for exhaust gas recirculation sweep at 1600 rpm and 50% load.

Figure 10 presents the averaged in-cylinder pressure traces for the DME EGR sweep conducted at 1600 rpm and 50% load. The figure includes EGR rates ranging from 22% to 55%. All conditions follow a similar compression trajectory prior to combustion, with the traces beginning to diverge as combustion initiates and proceeds through the expansion stroke. The 55% EGR case exhibits a higher-pressure curve throughout compression and early combustion because additional boost pressure was required to maintain the target operating condition. Figure 11 shows the AHRR traces for the DME EGR sweep at 1600 rpm and 50% load, with EGR rates ranging from 22% to 55%. As EGR increases, the onset of heat release remains similar, but the shape and magnitude of the main heat release event shift. Lower EGR cases (22–30%) exhibit higher peak AHRR and a sharper rise in heat

release, while higher EGR levels (40–55%) show reduced peak magnitudes and broader main combustion profiles.

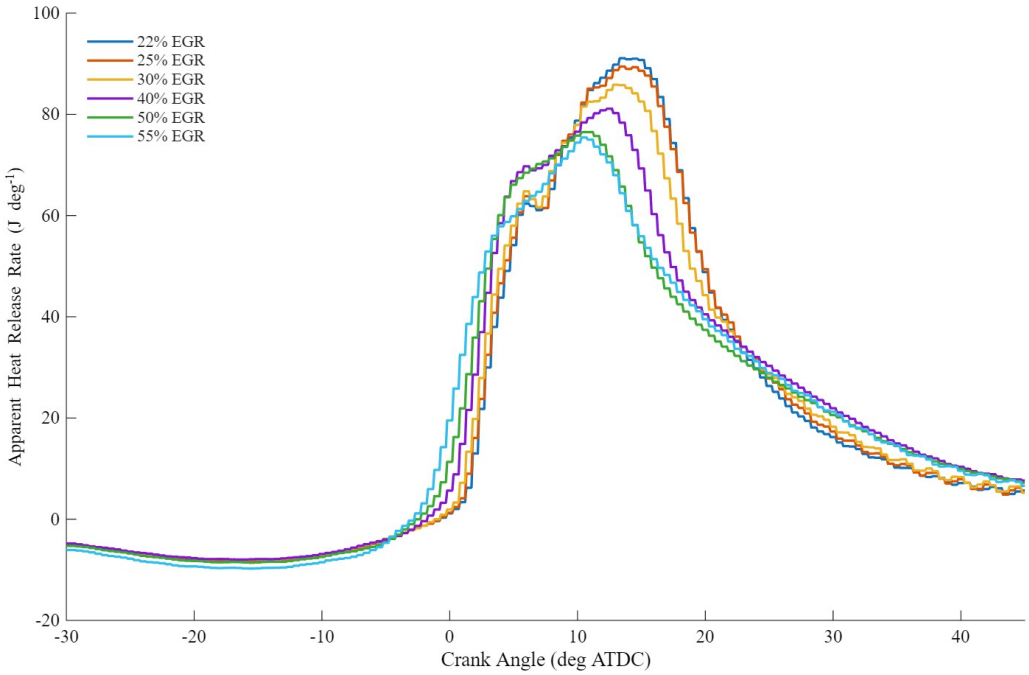

Figure 11. Apparent heat release rates for exhaust gas recirculation sweep at 1600 rpm 50% load.

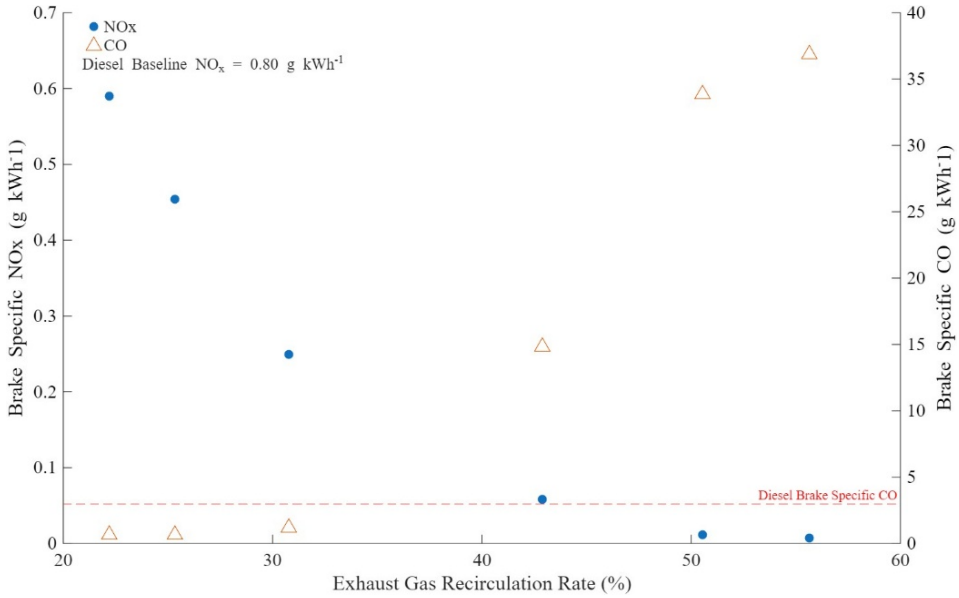

Figure 12. EGR rate vs. brake-specific nitrogen oxides and brake-specific carbon monoxide.

The duration for SOI–CA5 across the DME EGR sweep at 1600 rpm and 50% load shows a consistent increase as EGR rate rises, from 22% and SOI–CA5 of 12.96 deg to 55% and SOI–CA5 of 17.97 deg, with higher EGR rates corresponding to longer intervals between injection and the onset of combustion.

The CA10–90 across the DME EGR sweep at 1600 rpm and 50% load shows that CA10–90 increases as EGR rate rises from 22% and CA10–90 of 27.93 deg to 55% and CA10–90 of 32.89 deg, with higher EGR rates producing progressively longer burn durations across the sweep.

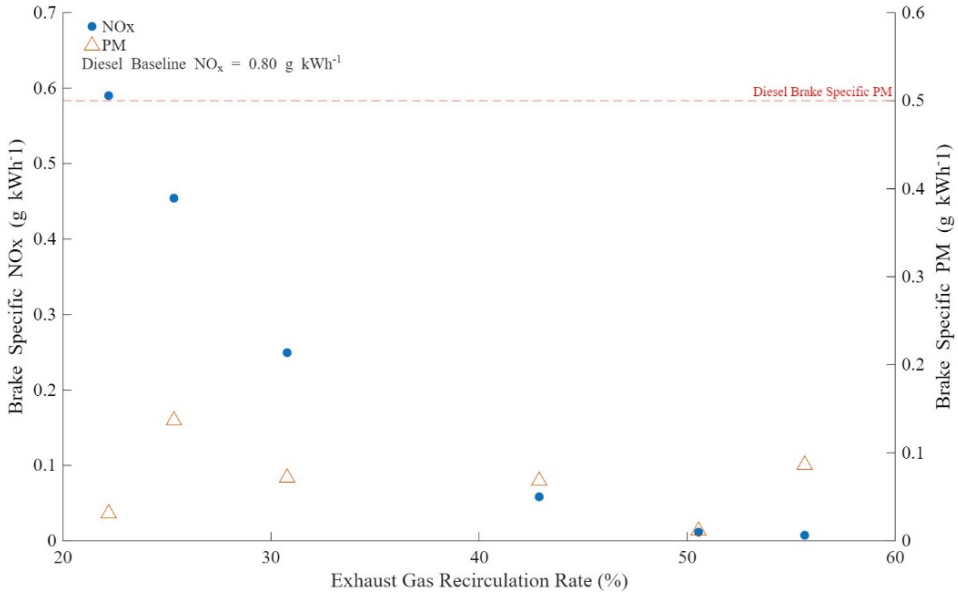

Figure 13. EGR rate vs. brake-specific nitrogen oxides and brake-specific particulate matter.

The effect of EGR dilution on DME combustion is shown in Figure 12, comparing $BSNO_x$ and BSCO as a function of EGR rate. NO_x decreases with increasing EGR. However, elevated EGR introduces incomplete oxidation behavior, visible in the rise of CO emissions at high EGR rates. This NO_x–CO tradeoff occurs around 40% EGR, where the levels of CO emissions are significantly higher than the baseline value for diesel.

BSPM remained consistently low throughout the sweep, staying below the diesel baseline value of 0.50 g kWh^{-1} and exhibiting only modest variation despite substantial changes in EGR rate, as shown in Figure 13. This stability in PM is notable, as increased EGR typically suppresses NO_x formation at the expense of soot production. However, PM did not increase as NO_x was reduced. Concurrently, NO_x decreased sharply with increasing EGR, falling from approximately 0.58 g kWh^{-1} at low EGR to near-zero levels beyond 50% EGR.

The EGR sweep expands the analysis by isolating the effects of dilution on combustion and emissions at the optimal CA50 found previously. Increasing EGR from 22% to 55% extends SOI–CA5 and CA10–90 due to reduced oxygen concentration, increased specific heat of the cylinder charge, and lower in-cylinder temperature [1,52]. However, combustion remains stable throughout the full EGR sweep, with both COV of IMEP and COV of CA50 staying within accepted stability limits. Although both metrics increase with higher dilution, the EGR sweep remained within these thresholds, with COV of IMEP staying under 3% and COV of CA50 remaining below 2.5%. Only the highest EGR points display rising variability, suggesting that misfire proximity is reached beyond 50% EGR. This trend is consistent with findings by Roh et al. (2018) [45], who showed that DME maintains relatively stable combustion over a wide EGR range, with instability emerging only at very high dilution. Smolec et al. (2017) [53] similarly reported that DME engines tolerate high dilution with stable oxidation chemistry compared to diesel, particularly because of DME's high reactivity and complete vaporization.

The heat release traces for the EGR sweep show decreasing peak magnitude and broader combustion intervals as dilution increases, reflecting lower in-cylinder temperatures and slower overall reaction rates. Even under these cooler and more diluted conditions, particulate emissions remain low across all EGR levels and consistently below the diesel baseline. This behavior aligns with the results of Smolec et al. (2017) [53] and Oda Yuji et al. (2004) [54], who reported essentially smoke-free or very low soot combustion

for DME in CI engines over a wide operating range. Fang et al. (2011) [13] showed that a heavy-duty DME-fueled engine can achieve simultaneously low NO_x and low smoke opacity up to about 40% EGR, with soot emission regions significantly smaller than for diesel due to DME's high oxygen content and absence of C–C bonds. The present data confirm that increasing EGR reduces NO_x without incurring a PM penalty.

At high dilution levels, additional tradeoffs emerge. When EGR exceeds approximately 40%, CO increases noticeably and rises above the diesel baseline threshold, marking the onset of incomplete oxidation caused by lower combustion temperatures and slower reaction kinetics. These increases likely reflect a combination of kinetic limitation, dilution-driven mixing degradation, and localized flame quenching, which cannot be separated quantitatively with the present measurements. Plots of emissions versus NO_x reveal a boundary near 0.1 g kWh^{-1} where, below this NO_x level, CO and THC begin to rise above diesel baseline levels, and BSFC increases noticeably. This threshold is consistent with DME low-temperature combustion (LTC) and high-EGR studies that report similar behavior. This behavior was reported by Fang et al. (2011) [13], who observed that high EGR in a DME-fueled heavy-duty engine reduces NO_x and smoke but eventually increases THC, CO, and BSFC once dilution becomes too strong. Beatrice et al. n.d. documented a similar pattern in diesel LTC experiments with clean, cooled EGR, showing that very high EGR effectively suppresses NO_x but leads to incomplete combustion and higher CO, THC, and fuel consumption penalties [55].

3.5. NO_x Tradeoffs

To evaluate how emissions interact across varying operating conditions, NO_x was plotted against CO, PM, THC, and fuel consumption. The data points plotted consist of all the operating points and fuels from this study and are represented in Figures 14 and 15.

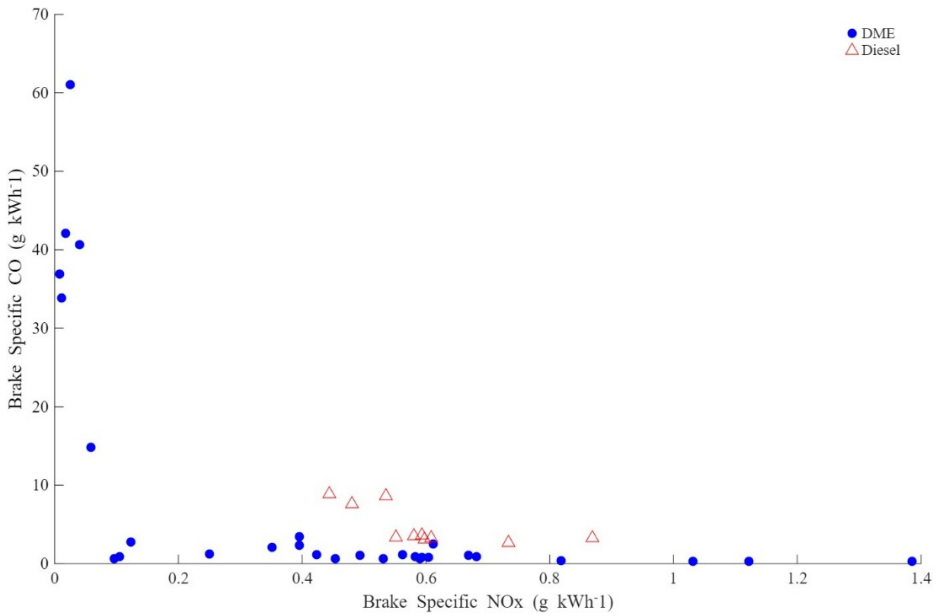

Figure 14. Brake-specific nitrogen oxides vs. brake-specific carbon monoxide.

In Figure 14, a clear NO_x–CO tradeoff is observed. CO remains relatively constant as NO_x decreases, with no notable rise in CO until NO_x levels drop below approximately 0.1 g kWh^{-1}. Above this threshold, CO emissions for DME remain lower than those of diesel at similar NO_x levels. THC emissions followed a trend similar to that of CO, with THC increasing as NO_x decreased. THC remains near zero and below diesel across most

of the NO_x range, and only begins to rise once NO_x drops below the same approximately 0.1 g kWh^{-1} threshold identified in the CO results.

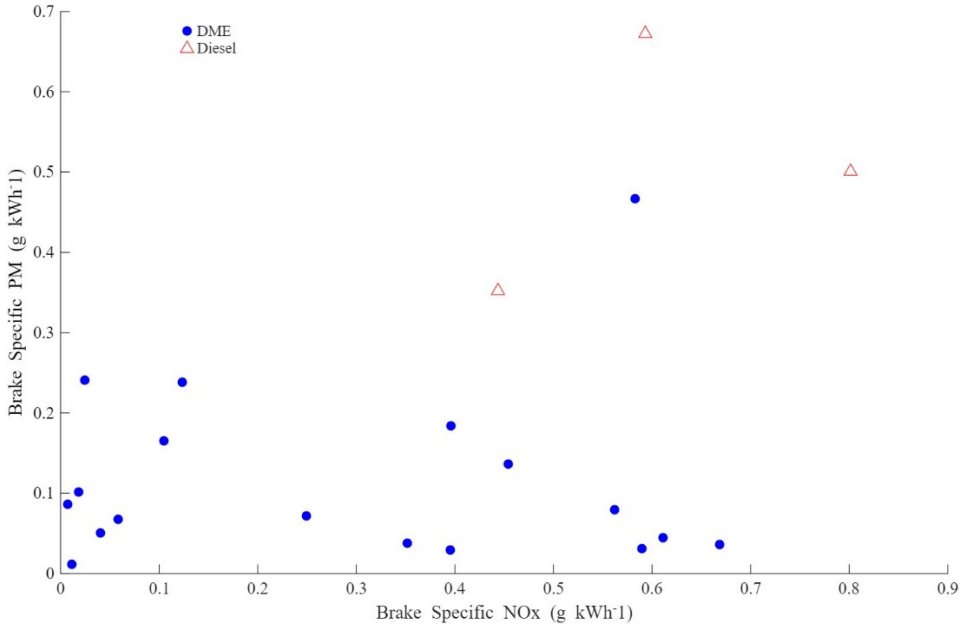

Figure 15. Brake-specific nitrogen oxides vs. brake-specific particulate matter.

Figure 15 shows a favorable PM–NO_x tradeoff. PM emissions remain low across the full NO_x range, suggesting that soot formation is largely independent of NO_x reduction strategies when using DME. In contrast, diesel produces higher PM at comparable NO_x values. One DME outlier exists, where PM rises to 0.47 g kWh^{-1} at a NO_x level of 0.58 g kWh^{-1}.

Brake-specific energy consumption (BSEC) increases as brake-specific NO_x decreases. A noticeable rise in BSEC occurs near the same 0.1 g kWh^{-1} NO_x threshold where THC and CO also increase. However, above this threshold, BSEC remains constant, with the exception of several points near 15 kJ kWh^{-1}. These elevated values correspond to the higher speed and load conditions at 2200 rpm and 50% and 75% load.

When the injection timing and EGR results are considered together, an optimal operating region emerges. Combustion phasing centered around a CA50 of approximately 16 deg ATDC and EGR rates between 30% and 40% provide a favorable balance of low NO_x, low PM, controlled CO and THC, stable combustion, and efficient fuel use. Within this region, the COV of IMEP and COV of CA50 remain well below stability thresholds, PM remains low, and NO_x is reduced without triggering the penalties seen at extremely low NO_x levels. Observed trends in prior DME CI studies support this identified optimum range.

Based on the combined results of the injection timing and EGR sweeps, the recommended operating condition for DME at 1600 rpm and 50% load is a combustion phasing near CA50 of 16 deg ATDC with an EGR rate between 30% and 40%. These values were selected because they represent the region where DME simultaneously achieves low NO_x, low PM, stable combustion, and acceptable efficiency without inducing the increases in CO, THC, and BSFC observed at higher dilution or more retarded phasing.

4. Conclusions

This study examined the feasibility of DME as a CI fuel capable of achieving low engine-out NO_x emissions while maintaining negligible PM and diesel-comparable brake power. The research began with the conversion of a John Deere 6068CI550 engine into a

fully instrumented SCRE, followed by baseline characterization on diesel and a series of controlled combustion experiments using DME. This study was completed in a manner that directly supported the overarching goal of understanding DME's soot–NO_x tradeoff and defining the limits of clean, stable combustion. Key takeaways for this study are below:

1. DME produced lower overall emissions than diesel while maintaining the diesel-equivalent IMEP, CA50, and EGR.
2. DME maintained thermal efficiency similar to that of diesel, despite higher mass-based BSFC.
3. Low NO_x and low PM occurred simultaneously with DME across the full EGR range tested (approximately 20–55%), demonstrating the absence of a diesel-like soot–NO_x tradeoff.
4. DME PM consisted almost entirely of organic carbon, with negligible elemental carbon measured across all operating points.
5. DME combustion remained stable up to 55% EGR with appropriate boost and fueling support.
6. At the tested condition of 1600 rpm and 50% load, optimal operating conditions were identified at CA50 of 16 deg ATDC and an EGR rate between 30% and 40%.
7. A combustion incompleteness threshold appeared below approximately 0.1 g kWh^{-1} NO_x, where CO, THC, and BSFC noticeably increased.

Future work should focus on refining the combustion boundary identified near 0.1 g kWh^{-1} NO_x, where CO, THC, and BSFC begin to increase and incomplete oxidation emerges. Higher resolution sweeps around this transition zone would clarify the mechanisms governing the onset of combustion instability and provide more precise calibration guidance. Additional testing at higher loads and speeds is needed to determine whether the optimal EGR region and phasing characteristics observed here persist across the broader operating map. Further investigation into multi-injection strategies, injection pressure effects, and alternative nozzle geometries may help suppress incomplete combustion products at ultra-low NO_x conditions.

Future studies should expand the current test matrix using multi-variable design of experiments and optimization methods to more efficiently identify globally optimal DME operating regions. Techniques such as the response surface methodology and the method of steepest ascent could be used to simultaneously vary injection timing, EGR rate, rail pressure, and boost to efficiently identify globally optimal operating regions. Future studies should also employ identical injector geometry and nozzle configuration across fuels, with only flow capacity scaled as required, to isolate fuel-property effects from injector-driven spray and mixing differences. This approach would directly quantify how control parameters interact and would allow identification of optimal tradeoff regions between emissions, fuel consumption, and combustion stability, supporting development of full DME calibration maps.

Beyond combustion optimization, practical considerations need attention. Longer-duration testing is required to evaluate DME pump, injector, and sealing reliability, and to ensure that fuel system materials can withstand DME's low lubricity. In addition, the feasibility of DME as a commercial diesel replacement depends heavily on expanding its production and distribution network, which remains limited today. Because of DME's lower LHV compared to diesel, larger onboard fuel storage capacity is required to achieve comparable operating duration, further emphasizing the need for supply and infrastructure development. Finally, CFD studies of DME evaporation, mixing, and ignition would help in interpreting the physical processes underlying the experimental results and guide future hardware and calibration strategies.

Author Contributions: Conceptualization, D.B.O.; Methodology, J.F.R., B.C.W. and D.B.O.; Validation, J.F.R.; Formal analysis, M.R.; Investigation, M.R., J.F.R. and D.B.O.; Data curation, M.R. and J.F.R.; Writing—original draft, M.R.; Writing—review & editing, J.F.R., B.C.W. and D.B.O.; Supervision, B.C.W. and D.B.O.; Project administration, D.B.O.; Funding acquisition, B.C.W. and D.B.O. All authors have read and agreed to the published version of the manuscript.

Funding: This work was funded by the US Department of Energy, Vehicle Technologies Office, award number DE-EE0011174.

Data Availability Statement: The original contributions presented in the study are included in the article, further inquiries can be directed to the corresponding author.

Conflicts of Interest: The authors declare no conflict of interest.

Abbreviations

The following abbreviations are used in this manuscript:

AHRR	Apparent Heat Release Rate
ASTM	American Society for Testing and Materials
ATDC	After Top Dead Center
BDC	Bottom Dead Center
BSCO	Brake-specific Carbon Monoxide
BSEC	Brake-Specific Energy Consumption
BSFC	Brake-Specific Fuel Consumption
$BSNO_x$	Brake-Specific Nitrogen Oxides
BSPM	Brake-Specific Particulate Matter
BSTHC	Brake-Specific Total Unburned Hydrocarbons
CA	Crank Angle
CA5	Crank Angle at 5% Mass Fraction Burned
CA10–90	Crank Angle Interval from 10% to 90% Mass Fraction Burned
CA50	Crank Angle at 50% Mass Fraction Burned
CI	Compression Ignition
CO	Carbon Monoxide
CO_2	Carbon Dioxide
COV	Coefficient of Variation
DME	Dimethyl Ether
DOC	Diesel Oxidation Catalyst
DOE	U.S. Department of Energy
DPF	Diesel Particulate Filter
EC	Elemental Carbon
EGR	Exhaust Gas Recirculation
FTIR	Fourier Transform Infrared Spectroscopy
HC	Hydrocarbons
IMEP	Indicated Mean Effective Pressure
ISO	International Organization for Standardization
LHV	Lower Heating Value
NI	National Instruments
NO_x	Nitrogen Oxides
OC	Organic Carbon
PM	Particulate Matter
SCRE	Single-Cylinder Research Engine
SOI	Start of Injection
TDC	Top Dead Center
THC	Total Unburned Hydrocarbons
ULSD	Ultra-Low Sulfur Diesel
VFD	Variable Frequency Drive

References

1. Heywood, J.B. *Internal Combustion Engine Fundamentals*; McGraw-Hill Book Company: New York, NY, USA, 1988; 930p.
2. J. E. Sinor Consultants Inc. *Fundamental Aspects of Dimethyl Ether*; Department of Energy: Washington, DC, USA, 1998.
3. Stepanenko, D.; Kneba, Z. DME as alternative fuel for compression ignition engines—A review. *Combust. Engines* **2019**, *177*, 172–179. [CrossRef]
4. Agarwal, A.K.; Kumar, V.; Valera, H.; Mukherjee, N.K.; Mehra, S.; Nene, D. Ultra-low soot/particulate emissions from a dimethyl ether-fueled agricultural tractor engine. *Fuel* **2024**, *356*, 129637. [CrossRef]
5. Kim, M.Y.; Bang, H.; Lee, C.S. Experimental Investigation of Spray and Combustion Characteristics of Dimethyl Ether in a Common-Rail Diesel Engine. *Energy Fuels* **2007**, *21*, 793–800. [CrossRef]
6. European Union. *REGULATION (EU) 2016/1628 of the European Parliament and of the Council—Of 14 September 2016-on Requirements Relating to Gaseous and Particulate Pollutant Emission Limits and Type-Approval for Internal Combustion Engines for Non-Road Mobile Machinery, Amending Regulations (EU) No1024/2012 and (EU) No 167/2013, and Amending and Repealing Directive 97/68/EC*; Publications Office of the European Union: Luxembourg, 2016.
7. Control of Emissions of Air Pollution from Nonroad Diesel Engines and Fuel. Available online: https://www.federalregister.gov/documents/2004/06/29/04-11293/control-of-emissions-of-air-pollution-from-nonroad-diesel-engines-and-fuel (accessed on 1 December 2025).
8. Zhang, J.J.; Huang, Z.; Wu, J.H.; Qiao, X.Q.; Fang, J.H. Combustion and performance of heavy-duty diesel engines fuelled with dimethyl ether. *Proc. Inst. Mech. Eng. Part D J. Automob. Eng.* **2008**, *222*, 1691–1703. [CrossRef]
9. Soltic, P.; Hilfiker, T.; Wright, Y.; Hardy, G.; Fröhlich, B.; Klein, D. The potential of dimethyl ether (DME) to meet current and future emissions standards in heavy-duty compression-ignition engines. *Fuel* **2024**, *355*, 129357. [CrossRef]
10. Youn, I.; Jeon, J. Combustion Performance and Low NO_x Emissions of a Dimethyl Ether Compression-Ignition Engine at High Injection Pressure and High Exhaust Gas Recirculation Rate. *Energies* **2022**, *15*, 1912. [CrossRef]
11. Sezer, İ. A review study on the use of dimethyl ether in diesel engines: Effects on CO_2 emissions. *MANAS J. Eng.* **2023**, *11*, 25–52. [CrossRef]
12. Yoon, S.H.; Han, S.C.; Lee, C.S. Effects of high EGR rate on dimethyl ether (DME) combustion and pollutant emission characteristics in a direct injection diesel engine. *Energies* **2013**, *6*, 5157–5167. [CrossRef]
13. Fang, Q.; Huang, Z.; Zhu, L.; Zhang, J.J.; Xiao, J. Study on low nitrogen oxide and low smoke emissions in a heavy-duty engine fuelled with dimethyl ether. *Proc. Inst. Mech. Eng. Part D J. Automob. Eng.* **2011**, *225*, 779–786. [CrossRef]
14. Dec, J.E. A Conceptual Model of Dl Diesel Combustion Based on Laser-Sheet Imaging. In Proceedings of the International Congress & Exposition, Detroit, MI, USA, 24 February 1997; SAE Technical Papers; SAE International: Warrendale, PA, USA, 1997. [CrossRef]
15. Hountalas, D.T.; Mavropoulos, G.C.; Binder, K.B. Effect of exhaust gas recirculation (EGR) temperature for various EGR rates on heavy duty DI diesel engine performance and emissions. *Energy* **2008**, *33*, 272–283. [CrossRef]
16. Deere, J. OMAL213158. 2013. Available online: http://manuals.deere.com/omview/OMAL213158_19/DX,FUEL1_19_20130617.html (accessed on 12 September 2025).
17. *Specification for Diesel Fuel*; ASTM International: West Conshohocken, PA, USA, 2024. Available online: http://www.astm.org/cgi-bin/resolver.cgi?D975-24A (accessed on 1 December 2025). [CrossRef]
18. Higher Calorific Values of Common Fuels: Reference & Data. Available online: https://www.engineeringtoolbox.com/fuels-higher-calorific-values-d_169.html (accessed on 8 May 2025).
19. Zhu, H.; Bohac, S.V.; Nakashima, K.; Hagen, L.M.; Huang, Z.; Assanis, D.N. Effect of fuel oxygen on the trade-offs between soot, NO_x and combustion efficiency in premixed low-temperature diesel engine combustion. *Fuel* **2013**, *112*, 459–465. [CrossRef]
20. Raeie, N.; Emami, S.; Karimi Sadaghiyani, O. Effects of injection timing, before and after top dead center on the propulsion and power in a diesel engine. *Propuls. Power Res.* **2014**, *3*, 59–67. [CrossRef]
21. Robert, C.Y.; Shahed, S.M. Effects of Injection Timing and Exhaust Gas Recirculation on Emissions from a D.I. Diesel Engine. In *Proceedings of the 1981 SAE International Fall Fuels and Lubricants Meeting and Exhibition*; SAE International: Warrendale, PA, USA, 1981.
22. Squibb, C.W.; Schock, H.; Vedula, R.; Stuecken, T. Analysis of Variations in Fuel Spray, Combustion, and Soot Production in an Optical Diesel Engine Operating under High Simulated Exhaust Gas Recirculation Operating Conditions. In *Proceedings of the SAE 2016 World Congress and Exhibition; SAE Technical Papers*; SAE International: Warrendale, PA, USA, 2016. [CrossRef]
23. Sezer, İ. Effects of dimethyl ether on cyclic variations in compression ignition engines. *Eurasian J. Sci. Eng. Technol.* **2025**, *6*, 121–135. [CrossRef]
24. Kanda, T.; Hakozaki, T.; Uchimoto, T.; Hatano, J.; Kitayama, N.; Sono, H. 2005-01-0378 PCCI Operation with Early Injection of Conventional Diesel Fuel. Available online: www.sae.org (accessed on 1 December 2025).

25. Besch, M.C.; Covington, A.N.; Johnson, D.; Fowler, N.; Heltzel, R. Effects of EGR Addition onto Combustion Stability and Alternator Performance Variability of a Small, Single-Cylinder Diesel Generator. In *Proceedings of the SAE/JSAE 2016 Small Engine Technology Conference & Exhibition*; SAE Technical Papers; SAE International: Warrendale, PA, USA, 2016. [CrossRef]
26. Oberon Fuels. *OberonFuels_rDME Spec Sheet—2025*; Oberon Fuels: San Diego, CA, USA, 2023.
27. Felipe, J.; Rueda, R.; Olsen, D.B.; Windom, B.; Baker, D.; Quinn, J. Expanding the Knock/Emissions Limits for the Realization of Ultra-Low Emissions, High-Efficiency Heavy-Duty Natural Gas Engines. Ph.D. Thesis, Colorado State University, Fort Collins, CO, USA, 2023.
28. L'Orange, C.; Neymark, G.; Carter, E.; Volckens, J. A high-throughput, robotic system for analysis of aerosol sampling filters. *Aerosol Air Qual. Res.* **2021**, *21*, 210037. [CrossRef]
29. Eileen Birch, M. *NIOSH Manual of Analytical Methods (NMAM)*, 4th ed.; U.S. Department of Health and Human Services, Public Health Service, Centers for Disease Control and Prevention, National Institute for Occupational Safety and Health: Cincinnati, OH, USA, 2003.
30. Hussain, J.; Palaniradja, K.; Natarajan, A.; Manimaran, R. Effect of Exhaust Gas Recirculation (EGR) on Performance and Emission of a Compression Ignition Engine with Staged Combustion (Insertion of Unburned Hydrocarbon). *Int. J. Energy Eng.* **2012**, *2*, 285–292. [CrossRef]
31. Desantes, J.M.; Galindo, J.; Guardiola, C.; Dolz, V. Air mass flow estimation in turbocharged diesel engines from in-cylinder pressure measurement. *Exp. Therm. Fluid Sci.* **2010**, *34*, 37–47. [CrossRef]
32. Zheng, M.; Reader, G.T.; Hawley, J.G. Diesel engine exhaust gas recirculation—A review on advanced and novel concepts. *Energy Convers. Manag.* **2004**, *45*, 883–900. [CrossRef]
33. Wang, Y.; Zhuang, Y.; Yao, M.; Qin, Y.; Zheng, Z. An experimental investigation into the soot particle emissions at early injection timings in a single-cylinder research diesel engine. *Fuel* **2022**, *316*, 123288. [CrossRef]
34. Vressner, A. *Studies on the Load Range of an HCCI Engine Using In-Cylinder Pressure, Ion Current and Optical Diagnostics*; Lund University: Lund, Sweden, 2003.
35. Persson, H. *Spark Assisted Compression Ignition, SACI*; Lund University: Lund, Sweden, 2008.
36. Kistler Group. *High-Temperature Pressure Sensor for Combustion Engine Measurements, Type 6052C, Datasheet No. 6052C_000-552e-03.24*; Kistler Group: Winterthur, Switzerland, 2006.
37. Arcoumanis, C.; Bae, C.; Crookes, R.; Kinoshita, E. The potential of di-methyl ether (DME) as an alternative fuel for compression-ignition engines: A review. *Fuel* **2008**, *87*, 1014–1030. [CrossRef]
38. Putrasari, Y.; Lim, O. Dimethyl Ether as the Next Generation Fuel to Control Nitrogen Oxides and Particulate Matter Emissions from Internal Combustion Engines: A Review. *ACS Omega* **2021**, *7*, 32–37. [CrossRef]
39. Wei, Y.; Wang, K.; Wang, W.; Liu, S.; Chen, X.; Yang, Y.; Bai, S. Comparison study on the emission characteristics of diesel- and dimethyl ether-originated particulate matters. *Appl. Energy* **2014**, *130*, 357–369. [CrossRef]
40. Lucas, S.P.; Zdanowicz, A.; Wolff, W.W.; Windom, B. Drop-In Performance of Propyl-and Butyl-Terminated Oxymethylene Ethers in a Compression Ignition Engine. *SAE Int. J. Fuels Lubr.* **2025**, *19*, 1–13. [CrossRef]
41. Reciprocating Internal Combustion Engines-Exhaust Emission Measurement-Part 1: Test-Bed Measurement Systems of Gaseous and Particulate Emissions Copyright Protected Document. 2020. Available online: https://standards.iteh.ai/catalog/standards/iso/4c414d60-cdef-4c95-a588-9691b16677bd/iso-8178-1-2020 (accessed on 1 December 2025).
42. U.S. Environmental Protection Agency. Determination of PEMS Measurement Allowances for Gaseous Emissions Regulated Under the Heavy-Duty Diesel Engine in-Use Testing Program: Revised Final Report (EPA420-R-08-005). Assessment and Standards Division, Office of Transportation and Air Quality. Prepared by Southwest Research Institute Under EPA Contract No. EP-C-05-018. 2008. Available online: https://downloads.regulations.gov/EPA-HQ-OAR-2004-0072-0085/content.pdf (accessed on 1 December 2025).
43. Song, J.; Huang, Z.; Qiao, X.; Wang, W. Performance of a controllable premixed combustion engine fueled with dimethyl ether. *Energy Convers. Manag.* **2004**, *45*, 2223–2232. [CrossRef]
44. Huang, Z.H.; Wang, H.W.; Chen, Y.; Zhou, L.B.; Jiang, D.M. Study of combustion characteristics of a compression ignition engine fuelled with dimethyl ether. *Proc. Inst. Mech. Eng. Part D J. Automob. Eng.* **1999**, *213*, 647–652. [CrossRef]
45. Roh, H.G.; Park, S.; Lee, C.S. Effect of Exhaust Gas Recirculation on the Combustion and Emissions of Dimethyl Ether in a Passenger Vehicle Diesel Engine. *J. Energy Eng.* **2018**, *144*, 04018061. [CrossRef]
46. Park, S.H.; Cha, J.; Lee, C.S. Reduction of the pollutant emissions from a diesel engine by the application of dimethyl ether (DME) and the control of the intake oxygen flow rate. *Energy Fuels* **2012**, *26*, 3024–3033. [CrossRef]
47. Teng, H.; McCandless, J.C.; Schneyer, J.B. Compression Ignition Delay (Physical + Chemical) of Dimethyl Ether—An Alternative Fuel for Compression-Ignition Engines. In *Proceedings of the SAE 2003 World Congress & Exhibition*; SAE Technical Papers; SAE International: Warrendale, PA, USA, 2003. [CrossRef]
48. Cung, K.D.; Moiz, A.A.; Zhu, X.; Lee, S.Y. Ignition Process and Flame Lift-Off Characteristics of dimethyl ether (DME) Reacting Spray. *Front. Mech. Eng.* **2021**, *7*, 547204. [CrossRef]

49. Jamrozik, A.; Tutak, W.; Gnatowska, R.; Nowak, Ł. Comparative analysis of the combustion stability of diesel-methanol and diesel-ethanol in a dual fuel engine. *Energies* **2019**, *12*, 971. [CrossRef]
50. Kim, M.Y.; Yoon, S.H.; Ryu, B.W.; Lee, C.S. Combustion and emission characteristics of DME as an alternative fuel for compression ignition engines with a high pressure injection system. *Fuel* **2008**, *87*, 2779–2786. [CrossRef]
51. Zhang, J.; Qiao, X.; Wang, Z.; Guan, B.; Huang, Z. Experimental investigation of low-temperature combustion (LTC) in an engine fueled with dimethyl ether (DME). *Energy Fuels* **2009**, *23*, 170–174. [CrossRef]
52. Turns, R.S. *An Introduction to Combustion Concepts and Applications*, 3rd ed.; McGraw Hill: New York, NY, USA, 2012; pp. 107–136.
53. Smolec, R.; Idzior, M.; Karpiuk, W.; Kozak, M. Assessment of the potential of dimethyl ether as an alternative fuel for compression ignition engines. *Combust. Engines* **2017**, *169*, 181–186. [CrossRef]
54. Yuji, O.; Shinnosuke, O.; Hiroyuki, U.; Koutaro, F. *Clean Combustion Technology in Diesel Engines Operated with Dimethyl Ether*; Mitsubishi Heavy Industries, Ltd.: Tokyo, Japan, 2004.
55. Beatrice, C.; Capaldi, P.; Del Giacomo, N.; Guido, C.; Lazzaro, M. The effect of 'clean and cold' EGR on the improvement of low temperature combustion performance in a single-cylinder research diesel engine. In Proceedings of the 31st Meeting of the Italian Section of the Combustion Institute, Torino, Italy, 17–20 June 2008. Available online: http://www.combustion-institute.it/proceedings/proc2008/data/papers/IV/IV-5.pdf (accessed on 1 December 2025).

Disclaimer/Publisher's Note: The statements, opinions and data contained in all publications are solely those of the individual author(s) and contributor(s) and not of MDPI and/or the editor(s). MDPI and/or the editor(s) disclaim responsibility for any injury to people or property resulting from any ideas, methods, instructions or products referred to in the content.